Chemical constituents of Antidesma bunius aerial parts and the anti-AGEs activity of selected compounds

Hieu Nguyen-Ngoc, Mostafa Alilou, Séverine Derbré, Patricia Blanchard, Giang Nam Pham, Duc Trong Nghiem, Pascal Richomme, Hermann Stuppner, Markus Ganzera

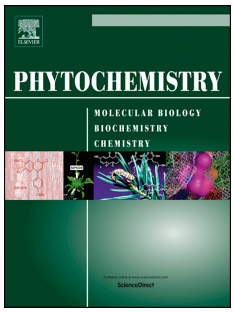

Chemical constituents of *Antidesma bunius* aerial parts and the anti-AGEs activity of selected compounds

Hieu Nguyen-Ngoc, Mostafa Alilou, Séverine Derbré, Patricia Blanchard, Giang Nam Pham, Duc Trong Nghiem, Pascal Richomme, Hermann Stuppner, Markus Ganzera

PII: S0031-9422(22)00216-3

DOI: https://doi.org/10.1016/j.phytochem.2022.113300

Reference: PHYTO 113300

To appear in: *Phytochemistry*

Received Date: 8 March 2022

Revised Date: 21 June 2022

Accepted Date: 27 June 2022

Please cite this article as: Nguyen-Ngoc, H., Alilou, M., Derbré, Sé., Blanchard, P., Pham, G.N., Nghiem, D.T., Richomme, P., Stuppner, H., Ganzera, M., Chemical constituents of *Antidesma bunius* aerial parts and the anti-AGEs activity of selected compounds, *Phytochemistry* (2022), doi: https://doi.org/10.1016/j.phytochem.2022.113300.

Graphical abstract

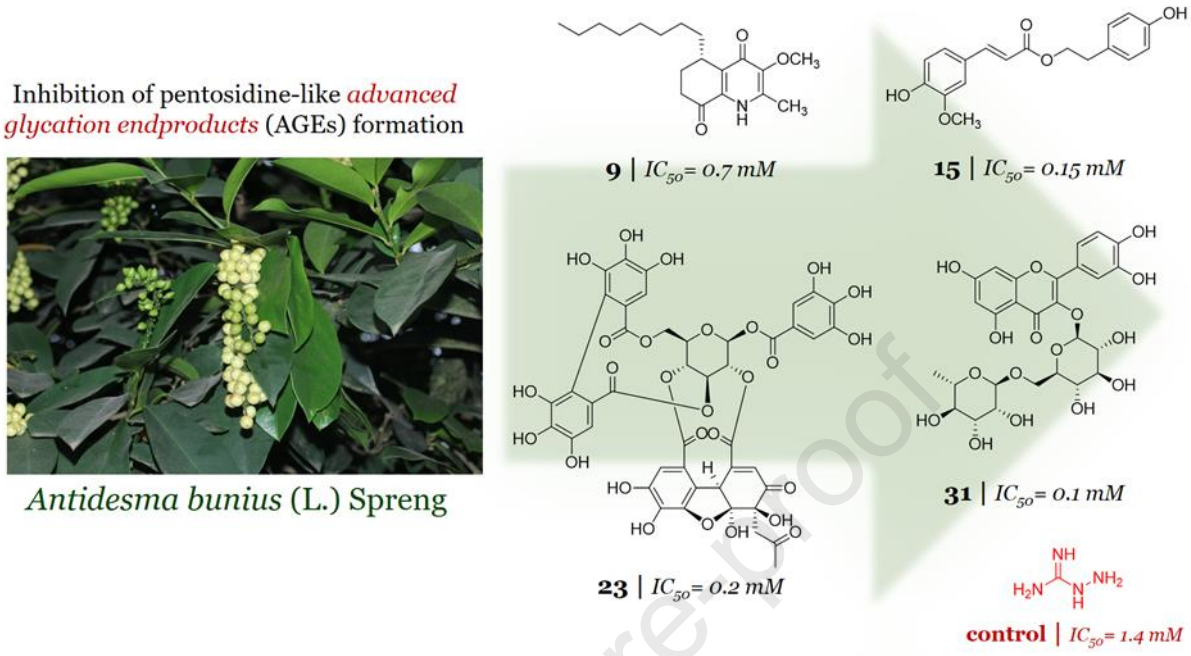

Chemical constituents of *Antidesma bunius* aerial parts and the anti-AGEs activity of selected compounds

Hieu Nguyen-Ngoc[a,b], Mostafa Alilou[a], Séverine Derbré[c], Patricia Blanchard[c], Giang Nam Pham[d], Duc Trong Nghiem[e], Pascal Richomme[c], Hermann Stuppner[a], Markus Ganzera[a,*]

[a] *Institute of Pharmacy, Pharmacognosy, Center for Molecular Biosciences (CMBI), University of Innsbruck, Innrain 80-82/IV, 6020 Innsbruck, Austria*

[b] *Faculty of Pharmacy, PHENIKAA University, Hanoi 12116, Vietnam*

[c] *SONAS, EA921, UNIV Angers, SFR QUASAV, Faculty of Health Sciences, Dpt Pharmacy, 16 Bd Daviers, 49045 Angers cedex 01, France*

[d] *College of Pharmacy, Chungnam National University, Daejeon 34134, Republic of Korea.*

[e] *Department of Botany, Hanoi University of Pharmacy, 13-15 Le Thanh Tong, Hoan Kiem, Hanoi 10000, Vietnam*

Corresponding Author

Markus Ganzera - *Institute of Pharmacy, Pharmacognosy, Center for Molecular Biosciences (CMBI), University of Innsbruck, Innrain 80-82/IV, 6020 Innsbruck, Austria*; https://orcid.org/0000-0002-7407-9060; Tel: +43-512-507-58406. Fax: +43-512-507-58499, E-mail: markus.ganzera@uibk.ac.at

Abstract

Thirty-three natural products were isolated from the aerial parts of *Antidesma bunius*, Euphorbiaceae, a plant used in Vietnamese traditional medicine against rheumatoid arthritis. All compounds were reported the first time for this species, and nine constituents resembled undescribed natural products, noticeably three coumarinolignans with 2,2-dimethyl-1,3-dioxolane moiety, two cyclopeptides, and two furofuran-type lignans connected with a phenylpropanoid moiety. The individual structures were elucidated by combining NMR and MS data, and their configuration was established by NOESY and ECD experiments and NMR calculations. Compounds with sufficient amount were analyzed for their inhibition of advanced glycation endproducts (AGEs) formation, metabolites involved in many diseases like Alzheimer, joint diseases or diabetes. With IC_{50} values below 0.2 mM rutin and *p*-hydroxyphenethyl *trans*-ferulate showed to be moderately active, both still being 10-times more active than the positive control aminoguanidine.

Keywords: *Antidesma bunius*, Euphorbiaceae, Cyclopeptide, Coumarinolignan, Advanced glycation endproducts

1. Introduction

Antidesma bunius (L.) Spreng. (Euphorbiaceae) is an up to 30 m tall tree, cultivated in high-precipitation areas of China and some Southeast Asian countries like Indonesia, Laos, Myanmar, Thailand, and Vietnam. In Java and the Philippines, its fruits are used as food, for preparing syrups, jams, jellies, and wine and liqueur production. The leaves are consumed as a vegetable and utilized in traditional medicine for the treatment of traumatic injury (eFloras, 2008). In Vietnam, the Dao ethnic community uses all plant parts to cure rheumatoid arthritis (Asia Foundation, 2012).

In 2016, Do et al. reported the isolation of two biflavones and three terpenoid glycosides from the methanolic extract of *A. bunius* leaves. The compounds displayed moderate inhibitory effects on NO production in BV2 cells and LPS-induced RAW264.7 macrophages (Trang et al., 2016). Mauldina and colleagues (2017) published a study on the bioactivity-guided isolation of natural products from *A. bunius* stem bark, which identified friedelin, β-sitosterol, and betulinic acid as potent α-glucosidase inhibitors (Mauldina et al., 2017). Other studies focused on pharmacological properties of *A. bunius* berries, indicating inhibition of the adipogenesis process and differentiation of adipocytes (Krongyut and Sutthanut, 2019), stimulation of fat metabolism in the liver (Ngamlerst et al., 2019), and a reduced formation of plaques in arteries (Tawali S et al., 2019). Besides, to the best of our knowledge, nothing else is known about the phytochemical composition of *A. bunius* aerial parts. Thus, in order to enable better insights into the constituents and pharmacological activity of this relevant medicinal plant, we have conducted the current investigation utilizing plant material collected in the Dao ethnic community of Ba Vi, Hanoi, Vietnam. Our efforts resulted in the isolation and identification of nine previously undescribed (**1**-**5**, **8**, **16**, **17**, and **20**) and 24 known (**6**, **7**, **9**-**15**, **18**, **19**, **21**-**33**) compounds. Some of the isolated compounds were then examined for their potential to inhibit the formation of advanced glycation endproducts (AGEs).

In the organism, AGEs result from the non-enzymatic reaction between simple sugars or their oxidized derivatives (i.e., 1,2-dicarbonyl compounds) with the primary amino group of certain amino acids to form a Schiff base as intermediate. It is irreversibly converted to a ketoamine, the so-called Amadori product, which can undergo further reactions involving dicarbonyl intermediates to finally give stable AGEs (Nagaraj et al., 1996; Ueno et al., 2003). The latter are inflammatory mediators involved in vascular complications of diabetes, as well as many chronic inflammatory diseases such as rheumatoid arthritis (Dariya and Nagaraju, 2020; De Groot et al., 2010). Preventing AGEs formation using natural products, herbal drugs

or food could help avoiding such disorders by stopping oxidation and/or trapping dicarbonyl species (Khan et al., 2020).

2. Results and discussion

2.1. Isolation and structural elucidation of compounds

Nine previously not reported (**1**-**5**, **8**, **16**, **17**, and **20**), along with 24 known (**6**, **7**, **9**-**15**, **18**, **19**, **21**-**33**) compounds, could be isolated from *A. bunius* leaves, and the corresponding structures were elucidated through extensive analysis of 1D and 2D NMR spectroscopic, and HRESIMS data. The absolute configuration of previously undescribed compounds was established by characteristic NMR shift values, electronic circular dichroism (ECD) calculations (**1**-**5**, and **8**), and other techniques, including GC-MS analysis for sugar identification (**20**) as well as $Rh_2(OCOCF_3)_4$-induced CD spectra (**16** and **17**) (Fig. 1).

Compound **1** was isolated as colorless oil. Its molecular formula $C_{32}H_{38}O_9$ was established by a HRESIMS ion peak at *m/z* 565.2424 ($[M-H]^-$, calcd for $C_{32}H_{37}O_9$, 565.2443), corresponding to 14 indices of hydrogen deficiency. The ^1H NMR spectrum showed the presence of an ABX-spin system [δ_H 6.94 (1H, dd, *J*= 1.8, 8.4 Hz), 6.91 (1H, d, *J*= 1.8 Hz), and 6.89 (1H, d, *J*= 8.4 Hz)], two aromatic singlet protons [δ_H 7.46 (1H, s) and 6.45 (1H, s)], two methoxy groups [δ_H 3.87 (3H, s) and 3.84 (3H, s)], and six methyl groups [δ_H 1.48 (6H, s), 1.38 (3H, s), 1.35 (3H, s), 0.97 (3H, s), and 0.72 (3H, s)]. The ^{13}C NMR revealed one esteric (δ_C 159.9), 14 aromatic and olefinic (in the range of 100-150 ppm), and four oxygenated signals (δ_C 65.4, 76.4, 79.5, and 80.3). The upfield-shifted esteric carbon at δ_C 159.9 suggested a coumarin scaffold. This prediction was supported by HMBC correlations of H-4 (δ_H 7.46)/ C-2 (δ_C 159.9), C-5 (δ_C 100.0), C-9 (δ_C 137.9); H-5 (δ_C 6.45)/ C-4 (δ_C 138.1), C-9; and by a comparison with published data (Chen et al., 2004; Chen et al., 2007). A 1,1-dimethylallyl fragment was indicated by two methyls [δ_H 1.48 (6H, s)] and three olefinic protons [δ_H 5.09 (1H, d, *J*= 12.0 Hz), 5.09 (1H, d, *J*= 17.4 Hz), and 6.18 (1H, dd, *J*= 10.2, 17.4 Hz)]. The 1,1-dimethylallyl moiety was determined to bind to C-3 by an HMBC correlation from H-12 (δ_H 1.48), H-13 (δ_H 1.48) to C-3 (δ_C 132.8), while methoxylation at C-6 was indicated by an HMBC correlation from OMe (δ_H 3.84) to C-6 (δ_C 145.7). An ABX-spin system, together with two downfield aromatic carbons at δ_C 146.5 and 146.9, and an HMBC correlation of OMe (δ_H 3.87)/ C-3′ (δ_C 146.9), was typical for the presence of a 3-methoxy-4-hydroxybenzene moiety. The structure of the side chain was elucidated based on HMBC and COSY correlations, as shown in Fig. 2. The two substructures were connected through 7-*O*-7′ and 8-*O*-8′ etheric bonds, which

were assured by key HMBC correlations of H-7′ (δ_H 5.22)/C-7 (δ_C 135.7) and H-8′ (δ_H 4.36)/C-8 (δ_C 132.0). The coupling constant (J= 5.4 Hz) of the two vicinal protons H-7′ and H-8′ indicated that they are *trans*-orientated (Bozzo et al., 2003; Chen et al., 2004). However, NOESY correlations did not allow the determination of the relative configuration at C-10′. Therefore, the planar structure of **1** was established as 2-(2-(2,2-dimethyl-1,3-dioxolan-4-yl)propan-2-yl)-3-(4-hydroxy-3-methoxyphenyl)-5-methoxy-8-(2-methylbut-3-en-2-yl)-2,3-dihydro-9H-[1,4]dioxino[2,3-h]chromen-9-one.

Compound **2** had the same molecular formula as **1**, which was indicated by a deprotonated ion peak at *m/z* 565.2419 ($[M-H]^-$, calcd for $C_{32}H_{37}O_9$, 565.2443) in the HRESI mass spectrum. NMR data of **2** were similar to **1**, except for C-7′, 8′, and 10′ (Table 1). The coupling constants of H-7′ and H-8′ were 6.6 Hz, which is typical for *trans*-conformation of the two protons (Bozzo et al., 2003; Chen et al., 2004). Again, the relative configuration of position C-10′ could not be established by NOESY. Thus, the planar structure of **2** was determined as 2-(2-((2,2-dimethyl-1,3-dioxolan-4-yl)propan-2-yl)-3-(4-hydroxy-3-methoxyphenyl)-5-methoxy-8-(2-methylbut-3-en-2-yl)-2,3-dihydro-9H-[1,4]dioxino[2,3-h]chromen-9-one.

Considering the presence of a 2,2-dimethyl-1,3-dioxolane group in compounds **1** and **2**, which can potentially be introduced while extraction/fractionation using acetone, an LC-MS analysis of the crude methanolic extract of *A. bunius* was performed for further confirmation (data not shown in detail). The obtained MS spectra in extracted ion chromatogram mode did not indicate the presence of **1** (MW: 526.58) or **2** (MW: 526.58) in the extract. Thus, it was concluded that these two compounds are artifacts. Nevertheless, also the original structures, i.e. those without the dioxolane group, were found to be previously undescribed natural products.

Both compounds shared the same planar structure, and the relative configuration of C-7′ and 8′ was determined to be *trans* (gauche), based on the previously mentioned coupling constants (lower ^3J coupling constants due to the gauche effect) and observed NOE from H-7′ to H-2′ in **1** and **2**. Moreover, these two compounds displayed different retention times on an achiral C-18 column, indicating diastereoisomers. Considering the observed mirror ECD spectra (Figure 3A), it can be concluded that the stereochemistry of C-10′ has to be the same in **1** and **2**, and the rest are to be mirror images of each other. To establish the relative configuration of C-10′, NMR chemical shift calculation followed by DP4+ probability calculation was implemented. Briefly, geometrical optimization and NMR calculation were performed at CPCM/mPW1PW91/6-31+G(d,p)/B3LYP/6-31G(d) basis set and level of theory in chloroform on two possible isomers: 1 (7′*R*,8′*R*,10′*R*) and 2 (7′*R*,8′*R*,10′*S*). Further DP4+ probability

calculation (Grimblat et al., 2015) using experimentally obtained chemical shifts of **1** indicated the presence of isomer 1 with a probability of 100% (Fig. S1.8, Supplementary data). Subsequent simulation of the ECD spectrum at CPCM/TD-DFT/cam-B3LYP/6-31+G(d,p)/B3LYP/6-31+G(d,p)/CPCM basis set and level of theory in acetonitrile resulted in a spectrum matching with that of compound **1**. Ultimately and based on the aforementioned data, the absolute configurations of compounds **1** and **2** were established as 7′*R*,8′*R*,10′*R* and 7′*S*,8′*S*,10′*R*, respectively. Both compounds (including their unmodified structures) are previously unreported natural products, and they were named buniusines A and B.

The molecular formula of **3** was evidenced by a dominant HRESIMS peak at *m/z* 589.2433 ([M+Na]$^+$, calcd for $C_{32}H_{38}O_9Na$, 589.2408), and its 1D-NMR data resembled those of **1** and **2**. However, a detailed analysis of the HMBC spectrum showed correlations of H-8′ (δ_H 4.36)/C-7 (δ_C 136.5) and H-7′ (δ_H 5.22)/C-8 (δ_H 131.2), indicating that compound **3** is a regional isomer of **1** and **2**. Moreover, LC-MS analysis again indicated that a 2,2-dimethyl-1,3-dioxolane moiety was introduced during the extraction process (data not shown in detail). The conformation of H-7′ and H-8′ was determined to be *trans*-type (gauche) by a coupling constant of 4.8 Hz (Bozzo et al., 2003; Chen et al., 2004) and NOE correlations between H-8′ and H-2′. To establish the relative configuration of C-10′ similar to **1** and **2**, the DP4+ probability calculation for two possible isomers (1: 7′*S*,8′*S*,10′*R* and 2: 7′*S*,8′*S*,10′*S*) was applied. The results confirmed isomer 2 with a probability of 99.83% to be the correct stereoisomer. Furthermore, using ECD calculation, the absolute configuration of compound **3** was established as 7′*S*,8′*S*,10′*S* (Fig. S3.8, Supplementary Data). Collectively, the structure of **3** was deduced as (2*S*,3*S*)-3-(2-((*S*)-2,2-dimethyl-1,3-dioxolan-4-yl)propan-2-yl)-2-(4-hydroxy-3-methoxyphenyl)-5-methoxy-8-(2-methylbut-3-en-2-yl)-2,3-dihydro-9H-[1,4]dioxino[2,3-h]chromen-9-one, a compound named buniusine C.

Buniusines A-C (**1**-**3**) belong to the class of coumarinolignans, which can be found in other *Antidesma* species, such as antidesmanins A-D in *A. pentandrum* root (Chen et al., 2004). The characteristic features of these natural products are a coumarin core connected with a phenylpropanoid moiety via two ether bonds. In addition, an 1,1-dimethylallyl moiety is often linked with C-3 of the coumarin core (Chen et al., 2007). Chen and colleagues (2004) reported the isolation and identification of two racemic mixtures of similar structures, antidesmanins C and D. However, due to small quantities of isolated compounds, their exact chemical structure could not be confirmed (Chen et al., 2004). In our study, compounds **1**-**3** might have been modified by acetone during the fractionation procedure. However, these changes permitted the

isolation of individual isomers on a conventional C-18 column, whose absolute configuration was then determined on the basis of ECD and NMR calculations.

Compound **4** was isolated as a yellowish amorphous powder. Its molecular formula could be established by a deprotonated ion peak at *m/z* 531.3018 ([M-H]$^-$, calcd for $C_{31}H_{39}N_4O_4$, 531.2977) in the HRESI mass spectrum. The ^{1}H NMR spectrum showed multiple signals in the aromatic range (δ_H 6.5-7.5 ppm), one N-methyl group [δ_H 2.22 (3H, s)], and four doublet methyl groups [δ_H 0.68 (3H, d, *J*= 6.6 Hz), 0.73 (3H, d, *J*= 6.6 Hz), 0.86 (3H, d, *J*= 6.6 Hz), and 1.14 (3H, d, *J*= 7.2 Hz)]. Three carbon signals in the range of δ_C 165-175 ppm were found; knowing that also four nitrogen atoms are present, this indicated three amide functionalities in the molecule. 1D and 2D NMR data analysis along with a comparison to literature values (Lomchoey et al., 2018) assigned these nitrogens to *p*-oxystyrylamine, 2-hydroxyleucine, phenylalanine, and 4-benzyl-3-methyl-5-oxoimidazolidine moieties, which strongly suggested the cyclopeptide alkaloid scaffold of **4**. *p*-Oxystyrylamine was identified by HMBC correlations from H-1 (δ_H 6.40) to C-13/14/15 (δ_C 131.6, 132.0, and 130.6, respectively) and from H-13 (δ_H 7.04) and H-15 (δ_H 7.03) to C-11. The presence of 2-hydroxyleucine and phenylalanine was confirmed by spin system H-6/H-5/H-17/H-18(H-19)/H-20 and H-8/H-9/H-21(H-22)/H-23, as well as HMBC correlations of H-5 (δ_H 4.04)/C-4 (δ_C 167.4), H-6 (δ_H 5.44)/C-7 (δ_C 168.3), and H-9 (δ_H 4.85)/C-7. As for the 4-benzyl-3-methyl-5-oxoimidazolidine moiety, COSY coupling networks of H-26/H-27 and H-31/H-32/H-33/H-34/H-35, along with a series of HMBC correlations of H-28 (δ_H 3.25 and 4.07)/C-25 (δ_C 172.4), C-26 (δ_C 67.5); N-Me (δ_H 2.22)/ C-26, C-28 (δ_C 68.4); and H-29 (δ_H 2.94 and 3.11)/C-30, C-31 (δ_C 137.2 and 130.2) confirmed its presence in **4**. The HMBC correlations of H-9 (δ_H 4.85)/C-11 (δ_C 156.1); H-5 (δ_H 4.04)/C-7 (δ_C 168.3); H-8 (δ_H 4.55)/C-25 (δ_C 172.4), C-28 (δ_C 68.4) indicated the connection of the four substructures, resulting in the planar structure of **4** as shown. Conformation of the double bond was *Z* because of the coupling constants of H-1 and H-2 (*J*= 9.6 Hz). The relative *erythro* configuration of C-8 and C-9 was deduced from a $^3J_{8,9}$ value of 7.8 Hz (Lomchoey et al., 2018). The NOESY spectrum displayed correlations between H-6 (NH) and H-8; H-6 and H-17 (but no correlations between H-6 and H-5); H-26 and H-18; a strong correlation between H-9 and H-28b (δ_H 4.07) and a weak correlation with H-28a (δ_H 3.25); and H-28 and H-9, conclusively resulting in deciphering the relative configuration of this structure as 5**S*,8**S*,9**S*,26**S*. Further calculation of the ECD spectrum indicated the absolute configuration of **4** as 5*S*,8*S*,9*S*,26*S*. From all deductions shown above, the structure of **4** was finally determined as (3*S*,4*S*,7*S*,*Z*)-4-((*S*)-4-benzyl-3-methyl-5-oxoimidazolidin-1-yl)-7-

isobutyl-3-isopropyl-2-oxa-6,9-diaza-1(1,4)-benzenacycloundecaphan-10-ene-5,8-dione, a previously undescribed natural product named buniusamide A.

Based on an HRESIMS signal at *m/z* 619.2909, the molecular formula of **5** was determined to be $C_{37}H_{40}N_4O_5$ ([M-H]$^-$, calcd for $C_{37}H_{39}N_4O_5$, 619.2926). ^{1}H and ^{13}C NMR spectra of this compound showed similarities to those of **4** (Table 2), indicating the same cyclopeptide scaffold. However, the ^{13}C NMR spectrum revealed four carbon signals in the range of δ_C 165-170 ppm, suggesting the molecule contains four amide groups. The presence of a *p*-oxystyrylamine moiety was assured by COSY coupling chains of H-15/H16; H-12/H-13; and H-1/H-2/H-3, as well as HMBC correlations from H-1/C-13, C-14, C-15 and from H-2/C-4. A 2-hydroxyphenylalanine moiety was determined by characteristic COSY coupling networks of H-21/H-22/H-23/H-24/H-25 and H-9/H-8/H-26, as well as key HMBC correlations from H-9 (δ_H 5.93)/C-20 (δ_C 137.5), C-21 (δ_C 128.4), C-25 (δ_C 128.4); and H-8 (δ_H 4.74)/C-7 (δ_C 170.6). A proline moiety was indicated by a coupling chain H-17/H-18/H-19/H-5 in the COSY spectrum and an HMBC correlation from H-5 (δ_H 3.85) to C-4 (δ_C 166.5). In addition to that, phenylalanine was also identified by two COSY coupling networks of H-31/H-32/H-33/H-34/H-35 and H-29/H-30/H-36, as well as an HMBC correlation of H-36 (δ_H 5.80)/C-27 (δ_C 170.9). These substructures could be connected by key HMBC correlations of H-2 (δ_H 6.74), H-5 (δ_H 3.85)/C-4 (δ_C 166.5); H-5/C-7 (δ_C 170.6); H-9 (δ_H 5.93)/C-11 (δ_C 155.5); and H-8 (δ_H 4.74)/C-27 (δ_C 170.9). Furthermore, a pentanamide moiety was identified by a COSY correlation chain [H-41/H-40(H-42)/H-39/H-38] and a typical HMBC crosspeak of H-38 (δ_H 5.64)/C-37 (δ_C 166.5). This moiety was linked to C-28, as evidenced by an HMBC crosspeak of H-28 (δ_H 4.54)/C-37 (δ_C 166.5). The double bond at C-38/C-39 had *E* type conformation (J = 15.0 Hz), whereas the relative configuration of 2-hydroxyphenylalanine was *trans* because of a coupling constant of J = 7.2 Hz (Caro et al., 2012). The NOESY spectrum was not helpful to deduce the relative configuration of other chiral centers at positions C-5 and C-28. Hence, DP4+ probability calculation was applied to reveal the relative configuration of **5**. The geometrical optimization followed by NMR chemical shift calculation was performed at CPCM/mPW1PW91/6-31+G(d,p)//B3LYP/6-31G(d) in chloroform for four possible diastereoisomers (isomer 1: 5*R*,8*S*,9*S*,28*S*, isomer 2: 5*S*,8*S*,9*S*,28*R*, isomer 3: 5*R*,8*S*,9*S*,28*R*, and isomer 4: 5*S*,8*S*,9*S*,28*S*), keeping in mind that the relative configuration of C-8 and C-9 is fixed (8**S*,9**S*). Further computation of DP4+ probability concluded isomer 2 (5*S*,8*S*,9*S*,28*R*) with a probability of 96.59% to be the correct stereoisomer (Fig. S5.8, Supplementary Data). The calculated ECD spectrum revealed to be opposite of the experimental one obtained in acetonitrile (Fig. 3E). Therefore, the structure of **5** was ultimately determined as (*E*)-*N*-((*S*)-1-

(((1^2*R*,8*R*,9*R*,*Z*)-2,10-dioxo-8-phenyl-7-oxa-3-aza-1(2,1)-pyrrolidina-6(1,4)-benzenacyclodecaphan-4-en-9-yl)amino)-1-oxo-3-phenylpropan-2-yl)-4-methylpent-2-enamide, a novel compound named buniusamide B.

Compound **8** showed a dominant deprotonated ion peak [M-H]$^-$ at *m/z* 334.2007 (cacld for $C_{19}H_{28}NO_4$, 334.2024) in the HRESI mass spectrum, which, together with the ^{13}C NMR data, indicated the molecular formula $C_{19}H_{29}NO_4$. ^{1}H NMR and HSQC spectra displayed signals assignable to amine [δ_H 8.79 (1H, s)], hydroxy [δ_H 6.86 (1H, s)], methoxy [δ_H 3.95 (3H, s)], and terminal methyl [δ_H 0.87 (3H, t, *J*= 6.6 Hz)] groups, as well as a methylene chain [δ_H 1.21-1.44 (m)]. The ^{13}C NMR spectrum showed characteristic resonances of an aliphatic ketone (δ_C 193.6), a conjugated ketone (δ_C 175.2), four olefinic carbons (δ_C 148.5, 139.3, 137.3, and 131.2), an oxygenated carbon (δ_C 72.7), a methoxy (δ_C 59.8), and an aliphatic chain (δ_C 14.2-38.1). Overall, 1D NMR data of **8** resembled that of antidesmone (**9**) (Bringmann et al., 2000a; Bringmann et al., 2000b), except for the presence of a carbon signal at δ_C 72.7. The position of this oxygenated carbon was located by HMBC correlations of H-11/C-5 (δ_C 72.7), C-6 (δ_C 32.4), C-10 (δ_C 137.5). Other key HMBC correlations for an antidesmone backbone were also found, specifically OMe (δ_H 3.95)/C-3 (δ_C 148.5), and 2-Me (δ_H 2.38)/C-2 (δ_C 139.3), C-3 (δ_C 148.5). NOESY crosspeaks of 2-Me (δ_H 2.38)/ OMe (δ_H 3.95) and NH (δ_H 8.79) supported the proposed planar structure. The absolute configuration at position C-5 was established to be *S* by ECD calculation with TD-DFT/cam-B3LYP/6-31G+(d,p)/CPCM (acetonitrile) functions (Fig. 3F). Collectively, the structure of **8** was elucidated as (*S*)-5-hydroxyantidesmone.

Compound **16** was isolated as white amorphous powder, its molecular formula $C_{41}H_{44}O_{14}$ established due to an *m/z* signal at 759.2651 ([M-H]$^-$, cacld for $C_{41}H_{43}O_{14}$, 759.2658). The ^{13}C NMR spectrum displayed 37 resonances, including one ester carbon, eight oxygenated aromatic carbons, sixteen aromatic carbons, nine oxygenated carbons, and three methoxy groups. With the HSQC spectrum and molecular formula it can be deduced that there was a symmetrical aromatic ring in the molecule. The COSY spectrum showed six coupling networks, specifically H-7/H-8[H-8′(H-9′)/H-7′]/H-9; H-5′/H-6′; H-5″/H-6″; H-7″/H-8″/H-9″; H-7‴/H-8‴; and H-5‴/H-6‴. HMBC correlations from H-7 (δ_H 4.74) to C-1 (δ_C 137.9), C-2 (δ_C 103.0); and from H-7′ (δ_H 4.76) to C-1′ (δ_C 132.9), C-2′ (δ_C 108.8), C-6′ (δ_C 119.1), as well as a comparison with reported ^{13}C NMR data from literature provided evidences for a medioresinol moiety (Xiong et al., 2011). A phenylpropanoid moiety was evidenced by a series of HMBC correlations of H-7″ (δ_H 4.89)/C-1″ (δ_C 130.9), C-2″ (δ_C 108.6), C-6″ (δ_C 119.0). In addition, couplings of H-7‴ (δ_H 7.51)/ C-1‴ (δ_C 127.2), C-2‴ (δ_C 109.4), C-6‴ (δ_C 123.2), and C-9‴ (δ_C 167.2) indicated the

presence of ferulic acid. The connection of these substructures was determined by crosspeaks of H-8″ (δ_H 4.56)/C-4 (δ_C 134.1) and H-9″ (δ_H 4.33 and 4.46)/C-9‴ (δ_C 167.2). HMBC correlations also facilitated location of the methoxyl groups as 3,5-OMe (δ_H 3.87)/C-3,5 (δ_C 153.8); 3′-OMe (δ_H 3.91)/C-3′ (δ_C 146.9); 3″-OMe (δ_H 3.92)/C-3″ (δ_C 146.9); and 3‴-OMe (δ_H 3.89)/C-3‴ (δ_C 146.8). Relative configuration of the medioresinol moiety was established by coupling constants of $^3J_{7,8}$ and $^3J_{7',8'}$ (4.8 Hz), as well as empirical rules of $\Delta\delta_{H\text{-}9,\ H\text{-}9'}$ (experimental data: 0.35 and 0.39 ppm; reference data: $\Delta\delta_{H\text{-}9,\ H\text{-}9'}$ for H-7/H-8 *trans*, H-7′/H-8′ *trans* 0.30-0.40 ppm; $\Delta\delta_{H\text{-}9,\ H\text{-}9'}$ for H-7/H-8 *cis*, H-7′/H-8′ *cis* <0.20 ppm) (Shao et al., 2018). The relative configuration of positions C-7″ and C-8″ of the phenylpropanoid moiety was of *erythro* type as evidenced by a small coupling constant of 3.6 Hz (Xiong et al., 2011), whereas configuration of the double bond between C-7‴ and C-8‴ was of *E*-type (*J*= 15.6 Hz). The medioresinol moiety was configured (7*R*,7′*R*,8*S*,8′*S*) due to a negative Cotton effect at 207 nm in the CD spectrum, which was comparable to that of (-)-acortatarinowin F and (-)-eudesmin (Lu et al., 2015). The 7″*R* configuration was evidenced by a negative Cotton effect at 345 nm (the E band) in the $Rh_2(OCOCF_3)_4$-induced CD spectrum of **16** (Fig. S7.7, Supplementary data) (Gerards and Snatzke, 1990; Xiong et al., 2011). Taking all observations together, the structure of **16** was established as (7*R*,7′*R*,7″*R*,8*S*,8′*S*,8″*S*)-9″-feruloyl-4′,4″-dihydroxy-3,3′,3″,5-tetramethoxy-7,9′:7′,9-diepoxy-4,8″-oxy-8,8′-sesquineolignan-7″-ol.

Compound **17** had the same molecular formula as **16** (*m/z* 759.2636, $[M\text{-}H]^-$, cacld for $C_{41}H_{43}O_{14}$, 759.2658). Also, 1D and 2D NMR data were in good agreement, suggesting that both compounds share the same lignan scaffold (Table 3). However, the coupling constant $^3J_{7'',8''}$ (8.4 Hz) indicated that compound **17** was the *threo* isomer of **16**. The relative configuration of the medioresinol moiety was established by coupling constants of $^3J_{7,8}$ and $^3J_{7',8'}$ (4.8 Hz), as well as by empirical rules of $\Delta\delta_{H\text{-}9,\ H\text{-}9'}$ data (experimental data: 0.36 and 0.37 ppm; reference data: $\Delta\delta_{H\text{-}9,\ H\text{-}9'}$ for H-7/H-8 *trans*, H-7′/H-8′ *trans* 0.30-0.40 ppm; $\Delta\delta_{H\text{-}9,\ H\text{-}9'}$ for H-7/H-8 *cis*, H-7′/H-8′ *cis* < 0.20 ppm) (Shao et al., 2018). A positive Cotton effect at 209 nm indicated the (7*S*,7′*S*,8*R*,8′*R*) configuration of the medioresinol moiety, which was opposite to that of **16**. The $Rh_2(OCOCF_3)_4$-induced CD spectrum method was applied to determine absolute configuration at position C-7″. The observed positive Cotton effect at 351 nm (E band), which again was opposite to **16**, indicated 7″*S* configuration (Fig. S8.7, Supplementary data). Collectively, the structure of **17** was (7*S*,7′*S*,7″*S*,8*R*,8′*R*,8″*S*)-9″-feruloyl-4′,4″-dihydroxy-3,3′,3″,5-tetramethoxy-7,9′:7′,9-diepoxy-4,8″-oxy-8,8′-sesquineolignan-7″-ol.

The molecular formula of **20** was established as $C_{28}H_{26}O_{18}$ by a HRESIMS signal at *m/z* 649.1051 ([M-H]$^-$, cacld for $C_{28}H_{25}O_{18}$, 649.1046). ^{1}H and ^{13}C NMR spectra of this compound displayed characteristic signals for a sugar moiety [δ_H 5.92 (1H, d, *J*= 8.4 Hz), 5.22 (1H, dd, *J*= 8.4, 9.6 Hz), 3.82 (1H, m), 3.62 (1H, t, *J*= 9.6 Hz), 3.86 (1H, m, H-5), 4.41 (1H, dd, *J*= 5.4, 12.0 Hz), 4.67 (1H, dd, *J*= 1.8, 12.0 Hz); δ_C 94.1, 74.2, 76.1, 71.7, 76.6, 64.6] and galloyl residues [δ_H 7.01 (2H, s), 7.05 (2H, s), 7.22 (1H, d, *J*= 1.8 Hz), 7.23 (1H, d, *J*= 1.8 Hz); δ_C 168.1, 167.6, 166.5]. Overall, shift values were very similar to 1,2,6-tri-*O*-galloyl-*β*-D-glucopyranose (Owen et al., 2003), except for split proton signals [δ_H 7.22 (1H, d, *J*= 1.8 Hz), 7.23 (1H, d, *J*= 1.8 Hz)] and an additional methoxy group [δ_H 3.89 (3H, s)]. Position of the latter was located by a HMBC cross-peak to C-3‴. The sugar was determined to be *β*-D-glucopyranose by a large coupling constant of the anomeric proton [δ_H 5.92 (1H, d, *J*= 8.4 Hz)], by NOESY correlations, and by comparing NMR data with the literature (Owen et al., 2003). GC-MS analysis of the hydrolysis product in comparison to authentic sugars also supported this conclusion. Therefore, the structure of **20** was determined as 1,2-di-*O*-galloyl-6-(3-methoxygalloyl)-*O*-*β*-D-glucopyranose.

The known compounds were identified as frangufoline (**6**) (Han et al., 1990), sanjoinenine (**7**) (Han et al., 1990), antidesmone (**9**) (Bringmann et al., 2000b), 17-*O*-(β-D-glucopyranosyl)antidesmone (**10**) (Buske et al., 2001), waltherione F (**11** (Cretton et al., 2014), aristolochic acid A (**12**) (Cai and Cai, 2010), α-linolenic acid (**13**) (Lee et al., 2016), linoleic acid (**14**) (Lee et al., 2016), *p*-hydroxyphenylethyl *trans*-ferulate (**15**) (Darwish and Reinecke, 2003), 5′-demethoxycarolignan Z (**18**) (Bouzergoune et al., 2016), syringaresinol (**19**) (An et al., 2016), 1,3,6-tri-*O*-galloyl-β-D-glucopyranose (**21**) (Yoshida et al., 1984), 1,2,4,6-tetra-*O*-galloyl-β-D-glucopyranose (**22**) (Tanaka et al., 1985), acetonylgranatin B (**23**) (Tanaka et al., 1992), acetonylhelioscopinin A (**24**) (Tanaka et al., 1992), acetonylterchebin (**25**) (Tanaka et al., 1992), acetonylcarpinusin (**26**) (Tanaka et al., 1992), 1-*O*-β-D-(2,4-dihydroxy-6-methoxyphenyl)-6-*O*-(4-hydroxy-3,5-dimethoxybenzoyl)-glucopyranose (**27**) (Bicker et al., 2009), 4-hydroxy-2-methoxyphenyl-6-*O*-syringoyl-β-D-glucopyranoside (**28**) (Hiltunen et al., 2006), mangiferin (**29**) (Martin et al., 2008), quercitrin (**30**) (Abdullaeva et al., 2016), rutin (**31**) (Kiyekbayeva et al., 2018), pectolinarin (**32**) (Peng, 2011), and vitexin (**33**) (Torres-Tapia et al., 2013) by comparing their NMR spectroscopic data with those reported in literature.

2.2. The anti-advanced glycation endproducts (AGE) activity of isolated compounds

As they were available in sufficient amount, fourteen of the isolated natural products were investigated for their anti-AGEs activity. The substances were evaluated in a concentration

range of 1 μM to 3 mM in comparison with the positive control (aminoguanidine: IC_{50} 1.4 mM). Among them, ellagitannins **23**-**26**, the phenylpropanoid **15**, and the quercetin glycosides **30**-**31** exhibited moderate inhibition of AGEs formation (Table 4). Rutin (**31**, IC_{50} 100 μM) has already been described as an AGEs inhibitor (Séro et al., 2013). Among the now tested compounds, *p*-hydroxyphenylethyl trans-ferulate (**15**), with two additional phenolic groups, was the second most potent inhibitor (IC_{50} 150 μM), still being ten times more active than the positive control. Also, the ellagitannins with IC_{50} values of 200 μM emerged as potential anti-AGEs, possibly due to many reducing phenolic groups in their structure. Indeed, using the same assay, many antioxidant polyphenols inhibited AGEs formation, most likely through their antioxidant potential (Rouger et al., 2015). As AGE formation is involved in many ailments, including joint diseases (Séro et al., 2013), this bioactivity might contribute to the traditional use of *A. bunius* against rheumatoid arthritis.

3. Conclusions

Phytochemical investigations on the aerial parts of *Antidesma bunius* led to the isolation and identification of 33 compounds, including nine previously undescribed compounds. Their planar chemical structures and absolute configurations were determined by a combination of ECD simulation, NMR calculation, and other chemical modification methods. The results revealed that *A. bunius* aerial parts contain unusual natural compound classes, such as cyclopeptides and coumarinolignans. The advanced glycation endproducts (AGE) inhibition bioassay was employed to evaluate bioactivity of some of the isolated compounds, in which rutin and *p*-hydroxyphenethyl *trans*-ferulate were the most active compounds with IC_{50} below 0.2 mM.

A. bunius is a popular medicinal plant in Asia, and the present study indicated that it is a source of structurally uncommon compounds, so that it definitely deserves more scientific attention in the future.

4. Experimental

4.1. General experimental procedures

Optical rotations were measured on a J-715 spectropolarimeter (Jasco, Japan) in a 10.0 cm tube, using the suitable solvent for each compound (MeOH or $CHCl_3$). IR spectra were

recorded on an Alpha FTIR spectrometer (Bruker), and ECD spectra on a J-1500 spectropolarimeter (JASCO, Japan). NMR experiments were carried out on an Avance II (600 MHz, Bruker, USA) using tetramethylsilane (TMS) as internal standard (Euriso-Top, France). HRESIMS spectra were recorded on a micrOTOF-Q II (Bruker) operated by Hystar software. For fractionation a Reveleris® system (Buchi, Switzerland) with detection wavelengths always set to 205, 254, and 280 nm, or open columns filled with silica-gel, RP-18 material or Sephadex LH-20 (Sigma-Aldrich, USA) were used. Final purifications were sometimes conducted on a semi-preparative Dionex HPLC system, equipped with a P580 pump, ASI 100 automated sample injector, UVD 170 U detector, and Gilson Ambimed 206 fraction collector, using a Phenomenex Synergi 4u MAX-RP 80A column (250 × 10 mm, 4 μm particle size). The flow rate was always set at 2.00 mL/min. All solvents required for extraction and isolation were purchased from VWR (Austria). Ultrapure water was produced by a Sartorius arium 611 UV system (Germany).

4.2. Plant material

Antidesma bunius (L.) Spreng. (Euphorbiaceae) aerial parts were collected in Ba Vi, Hanoi, Vietnam (GPS: 21˚03'60.0"N, 105˚20'3.0"E) in January 2018. The sample was authenticated by M.Sc. Duc Trong Nghiem from the Department of Botany, Hanoi University of Pharmacy, Hanoi, Vietnam. A voucher specimen (2018/01-AB) is deposited at the Institute of Pharmacy/ Pharmacognosy, University of Innsbruck, Innsbruck, Austria.

4.3. Extraction and isolation

The dried and powdered aerial parts of *A. bunius* (0.9 kg) were extracted with MeOH (2 L × 3 times × 2h) in an ultrasonic bath, and the combined extracts were evaporated under reduced pressure to obtain 80.3 g of green residue. The crude extract was suspended in distilled water (1 L), and then partitioned with EtOAc and *n*-BuOH (each 1 L × 3 times). The organic solvent layers were evaporated *in vacuo* to obtain respective portions.

The EtOAc-soluble extract (22.3 g) was fractionated on a silica gel column (8 × 15 cm, 40-63 μm), eluting with a gradient of petroleum ether (PE) and acetone (from 20:1 to 0:1), which resulted in 16 fractions (ABE 1-16). Fraction ABE 4 (1.5 g) was further purified on a normal-phase silica gel flash column (40 g NP cartridge, 0-50 min: 0-10% acetone in PE, 50-90 min: 10-20% acetone in PE, flow rate 8 mL/min), to obtain subfractions ABE 4.1-3. Fraction ABE 4.1 was subjected to a C_{18} flash column (12 g RP cartridge, 0-50 min: 60-85% MeOH, 50-85 min: 85-90% MeOH, flow rate 10 mL/min) to yield compounds **13** (11.0 mg) and **14** (41.6 mg). Fraction ABE 10 (0.3 g) was also further fractionated using a 12g C_{18} cartridge (0-

40 min: 80-100% MeOH, 40-65 min: 100% MeOH, flow rate 7 mL/min) to obtain subfractions ABE 10.1-4. Preparative HPLC was employed to purify subfractions ABE 10.3 (52 mg, 0-30 min: 55-70% CH_3CN) and 10.4 (44 mg, 0-35 min: 65-80% CH_3CN) to yield in compounds **8** (1.4 mg) and **11** (4.0 mg), respectively. Fraction ABE 11 (0.5 g) was separated by flash chromatography (12g C_{18} cartridge, 0-40 min: 30-60% MeOH, 40-85 min: 60-85% MeOH, 85-105 min: 85-90% MeOH, flow rate 8 mL/min) to afford subfractions ABE 11.1-4. Fraction ABE 11.3 (75 mg), which revealed four major peaks in the HPLC chromatogram, was purified by preparative HPLC, using 65% CH_3CN as eluent, to obtain compounds **1** (2.1 mg), **2** (1.5 mg), **3** (1.2 mg), and **9** (1.5 mg). Fraction ABE 12 (0.6 g) was first fractionated on a flash column (12 g RP cartridge, 0-40 min: 40-70% MeOH, 40-80 min: 70-100% MeOH, flow rate 8 mL/min). Fraction ABE 12.3 (0.3 g) was selected for further purification using size-exclusion chromatography (Sephadex LH-20, MeOH as eluent, 1 × 35 cm), resulting in subfractions ABE 12.3.1-6. By preparative HPLC, compounds **4** (1.5 mg), **5** (1.6 mg), and **7** (2.4 mg) from ABE 12.3.3 (63 mg, 0-40 min: 55-85% CH_3CN), as well as compound **12** (2.3 mg) from ABE 12.3.6 (32 mg, 0-30 min: 45-56% CH_3CN) could be obtained. Another fraction, ABE 14 (1.2 g), was separated on a RP-C_{18} flash column (12 g RP cartridge, 0-40 min: 30-65% MeOH, 40-60 min: 65-80% MeOH, flow rate 8 mL/min) to obtain seven subfractions (ABE 14.1-7). Subfraction ABE 14.4 (85 mg) was purified by preparative HPLC (0-24 min: 30-40% CH_3CN) to yield compounds **15** (24.7 mg) and **19** (2.8 mg). In the acetone solution of ABE 14.7 a white precipitate appeared. It was removed by centrifugation and washed with cold acetone to obtain compound **6** (5.0 mg); the remaining solution was subjected to a Sephadex LH-20 column (1 × 35 cm, CH_2Cl_2 : acetone = 85:15 as eluent). Out of the seven subfractions collected, compounds **16** (2.1 mg) and **17** (1.6 mg) were isolated by prep. HPLC (0-40 min: isocratic 40% CH_3CN) from ABE 14.7.5 (48 mg); subfraction ABE14.7.7 (55 mg) yielded compound **18** (0-30 min: 47-56% CH_3CN). Next, ABE 16 (4.2 g) was fractionated by Reveleris flash chromatography (80 g RP cartridge, 0-30 min: 5-30% MeOH, 30-110 min: 30-80% MeOH, flow rate 15 mL/min) into subfractions ABE 16.1-8. ABE 16.3 (1.3 g) was further separated on a Sephadex LH-20 column (1 × 35 cm, MeOH) into seven subfractions (ABE 16.3.1-7). Based on HPLC analysis, ABE 16.3.5 and ABE 16.3.7 were chosen for further purification. Subfraction ABE 16.3.5 (0.3 g) was subjected to a smaller RP-C18 flash column (12 g RP cartridge, 0-50 min: 10-20% ACN, 50-70 min: 20-25% MeOH, flow rate 7 mL/min) to obtain compound **21** (6.7 mg), and fraction ABE 16.3.5.4 (60 mg) was purified by preparative HPLC (0-35 min: 15-24% CH_3CN) to yield compounds **20** (3.1 mg) and **24** (3.1 mg). Subfraction ABE 16.3.7 (0.3 g) was first resolved by flash chromatography (12 g RP cartridge, 0-50 min: 10-20% CH_3CN, 50-70 min: 20-22%

CH_3CN, flow rate 7 mL/min), before being subjected to preparative HPLC (0-35 min: 18-23 % CH_3CN), to afford compounds **22** (2.1 mg), **23** (3.8 mg), and **26** (5.0 mg). Additionally, fractions ABE 16.4 (0.3 g) and ABE 16.5 (0.4 g) were purified by Sephadex LH-20 (1 × 35 cm, MeOH as eluent) to obtain compounds **25** (29.7 mg) and **27** (14.5 mg), as well as compound **30** (6.1 mg).

The *n*-BuOH soluble part (19.6 g) was initially fractionated on an open silica gel column (8 × 15 cm, 40-63 μm), using stepwise gradient elution with EtOAc and MeOH (ratio from 20:1 to 0:1) to obtain 10 fractions (ABB 1-10). Fraction ABB 3 (1.2 g) was separated by flash chromatography (12 g RP cartridge, 0-50 min: 10-50% MeOH, 50-90 min: 50-75% MeOH, flow rate 10 mL/min), and then compound **28** (2.9 mg) purified using Sephadex LH-20 material (1 × 35 cm column, MeOH). Fraction ABB 5 (1.5 g) was first divided into 11 subfractions (ABB 5.1-11) on a C_{18} Reveleris column (12 g RP cartridge, 0-50 min: 10-50% MeOH, 50-85 min: 50-80% MeOH, flow rate 10 mL/min). Subfraction ABB 5.7 (0.5 g) was submitted to a Sephadex LH-20 column (1 × 35 cm, MeOH) to obtain five further fractions (ABB 5.7.1-5). In the methanolic solution of ABB 5.7.4, white crystals formed at the bottom of vial. They were filtered and washed with cold MeOH to yield compound **29** (2.1 mg). Subfraction ABB 5.8 was purified by Sephadex LH-20 column chromatography (1 × 35 cm, MeOH), before compound **33** (1.6 mg) could be isolated by preparative HPLC (0-30 min: 15-24 % CH_3CN). Subfraction ABB 5.11 (0.1 g) was also purified using preparative HPLC (0-30 min: 25-34 % CH_3CN) to obtain compound **32** (1.6 mg). Another fraction, ABB 7 (1.2 g), was initially fractionated by flash chromatography (12 g RP cartridge, 0-50 min: 10-50% MeOH, 50-90 min: 50-80% MeOH, flow rate 10 mL/min), then on Sephadex LH-20 material (1 × 35 cm, MeOH), and finally subjected to preparative HPLC (0-31 min: 13-22 % CH_3CN), resulting in the isolation of compound **31** (2.3 mg). The same approach was utilised to isolate compound **10** (6.2 mg) from fraction ABB 8 (1.3 g), however using a slightly modified HPLC gradient (0-35 min: 20-30 % CH_3CN).

*4.3.1. Buniusine A (**1**)*

White amorphous powder; $[\alpha]_D^{20}$ +81.0 (*c* 0.05, $CHCl_3$); UV (CH_2Cl_2) λ_{max} (log ε) 228 (4.42), 321 (4.05) nm; ECD (CH_3CN) λmax (Δε) 192 (+6.21), 210 (-2.11), 221 (-4.82), 249 (+3.88), 279 (-2.71), 326 (+6.66); IR ν_{max} 3414, 2927, 1712, 1397, 1121, 1033, 734 cm^{-1}; ^1H and ^{13}C NMR data, see Table 1; HRESIMS *m/z* 565.2424 $[M-H]^-$ (calcd for $C_{32}H_{37}O_9$, 565.2443).

*4.3.2. Buniusine B (**2**)*

White amorphous powder; $[\alpha]_D^{20}$ -11.3 (*c* 0.08, $CHCl_3$); UV (CH_2Cl_2) λ_{max} (log ε) 228 (4.21), 323 (3.82) nm; ECD (CH_3CN) λmax (Δε) 206 (+3.76), 215 (+1.90), 246 (-3.59), 281 (+3.28), 325 (-3.83); IR ν_{max} 3434, 3393, 2927, 2822, 1397, 1139, 1064, 734 cm^{-1}; ^1H and ^{13}C NMR data, see Table 1; HRESIMS *m/z* 565.2419 $[M-H]^-$ (calcd for $C_{32}H_{37}O_9$, 565.2443).

*4.3.3. Buniusine C (**3**)*

White amorphous powder; $[\alpha]_D^{20}$ -19.5 (*c* 0.06, $CHCl_3$); UV (CH_2Cl_2) λ_{max} (log ε) 227 (4.21), 323 (3.81) nm; ECD (CH_3CN) λmax (Δε) 206 (+4.04), 214 (+6.67), 238 (-3.61), 309 (-5.20); IR ν_{max} 3393, 2925, 1710, 1397, 1137, 1065, 735 cm^{-1}; ^1H and ^{13}C NMR data, see Table 1; HRESIMS *m/z* 589.2433 $[M+Na]^+$ (calcd for $C_{32}H_{38}O_9Na$, 589.2408).

*4.3.4. Buniusamide A (**4**)*

Yellowish amorphous powder; $[\alpha]_D^{20}$ -188.9 (*c* 0.08, $CHCl_3$); UV (CH_2Cl_2) λ_{max} (log ε) 228 (4.52); ECD (CH_3CN) λmax (Δε) 200 (-16.62), 212 (+9.06), 243 (-26.38); IR ν_{max} 3391, 3292, 3052, 3032, 1673, 1451, 1183, 732, 697 cm^{-1}; ^1H and ^{13}C NMR data, see Table 2; HRESIMS *m/z* 531.3018 $[M-H]^-$ (calcd for $C_{31}H_{39}N_4O_4$, 531.2977).

*4.3.5. Buniusamide B (**5**)*

White amorphous powder; $[\alpha]_D^{20}$ -61.0 (*c* 0.08, $CHCl_3$); UV (CH_2Cl_2) λ_{max} (log ε) 227 (4.42); ECD (CH_3CN) λmax (Δε) 203 (-5.44), 217 (+7.09), 239 (-45.73); IR ν_{max} 3391, 3291, 2958, 2926, 1656, 1621, 1599, 1417, 1227, 732, 697 cm^{-1}; ^1H and ^{13}C NMR data, see Table 2; HRESIMS *m/z* 619.2909 $[M-H]^-$ (calcd for $C_{37}H_{39}N_4O_5$, 619.2926).

*4.3.6. 5S-hydroxyantidesmone (**8**)*

White amorphous powder; $[\alpha]_D^{20}$ +8.1 (*c* 0.07, $CHCl_3$); UV (CH_2Cl_2) λ_{max} (log ε) 247 (4.16), 336 (3.47) nm; ECD (CH_3CN) λmax (Δε) 211 (+12.50), 232 (-23.93), 316 (-10.71), 353 (+24.53), 367 (+24.80); IR ν_{max} 3217, 2923, 2853, 1698, 1611, 1548, 1271, 1165 cm^{-1}; ^1H NMR ($CDCl_3$, 600 MHz) δ_H 2.16 (1H, m, H-6a), 2.37 (1H, m, H-6b), 2.59 (1H, ddd, *J*= 4.2, 15.0, 18.6 Hz, H-7a), 2.76 (1H, ddd, *J*= 3.0, 4.2, 18.6 Hz, H-7b), 1.71 (1H, m, H-11a), 2.12 (1H, m, H-11b), 1.41 (1H, m, H-12a), 1.68 (1H, m, H-12b), 1.31 (2H, m, H-13), 1.28 (2H, m, H-14), 1.29 (2H, m, H-15), 1.25 (2H, m, H-16), 1.28 (2H, m, H-17), 0.87 (3H, t, *J*= 6.6 Hz, H-18), 3.95 (3H, s, OMe), 6.86 (1H, s, OH), 8.79 (1H, s, NH); ^{13}C NMR ($CDCl_3$, 150 MHz) δ_C 139.3 (C-2), 148.5 (C-3), 175.2 (C-4), 72.7 (C-5), 32.4 (C-6), 34.3 (C-7), 193.6 (C-8), 131.2 (C-9),

137.5 (C-10), 38.1 (C-11), 23.9 (C-12), 30.2 (C-13), 29.7 (C-14), 29.4 (C-15), 32.0 (C-16), 22.8 (C-17), 14.2 (C-18), 14.9 (2-Me), 59.8 (3-OMe); HRESIMS *m/z* $[M-H]^-$ 334.2007 (calcd for $C_{19}H_{28}NO_4$, 334.2024).

*4.3.7. (7R,7'R,7"R,8S,8'S,8"S)-9"-feruloyl-4',4"-dihydroxy-3,3',3",5-tetramethoxy-7,9':7',9-diepoxy-4,8"-oxy-8,8'-sesquineolignan-7"-ol (**16**)*

White amorphous powder; $[\alpha]_D^{20}$ +1.2 (*c* 0.05, $CHCl_3$); UV (CH_2Cl_2) λ_{max} (log ε) 228 (4.56), 286 (4.27), 320 (4.28) nm; IR ν_{max} 3444, 2926, 2853, 1700, 1634, 1514, 1267 cm^{-1}; ECD (CH_3CN) λmax (Δε) 208 (-1.44), 220 (+1.19), 230 (-1.23), 245 (+4.50), 292 (+2.74), 324 (+2.50); ^1H and ^{13}C NMR data, see Table 3; HRESIMS *m/z* 759.2651 $[M-H]^-$ (calcd for $C_{41}H_{43}O_{14}$, 759.2658).

*4.3.8. (7S,7'S,7"S,8R,8'R,8"S)-9"-feruloyl-4',4"-dihydroxy-3,3',3",5-tetramethoxy-7,9':7',9-diepoxy-4,8"-oxy-8,8'-sesquineolignan-7"-ol (**17**)*

White amorphous powder; $[\alpha]_D^{20}$ +2.5 (*c* 0.08, $CHCl_3$); UV (CH_2Cl_2) λ_{max} (log ε) 228 (4.56), 285 (4.29), 320 (4.31) nm; IR ν_{max} 3445, 2929, 2853, 1702, 1633, 1592, 1265, 1123, 1055, 733, 701 cm^{-1}; ECD (CH_3CN) λmax (Δε) 209 (+3.83), 231 (+0.36); ^1H and ^{13}C NMR data, see Table 3; HRESIMS *m/z* 759.2636 $[M-H]^-$ (calcd for $C_{41}H_{43}O_{14}$, 759.2658).

*4.3.9. 1,2-di-O-galloyl-6-(3-methoxygalloyl)-O-β-D-glucopyranose (**20**)*

Brownish gum; $[\alpha]_D^{20}$ -52.4 (*c* 0.05, MeOH); UV (MeOH) λ_{max} (log ε) 218 (4.61), 277 (4.24) nm; IR ν_{max} 3252 (br), 2947, 2840, 1700, 1606, 1317, 1194, 1005, 760 cm^{-1}; ^1H NMR (MeOH-d_4, 600 MHz) δ_H 5.92 (1H, d, *J*= 8.4 Hz, H-1), 5.22 (1H, dd, *J*= 8.4, 9.6 Hz, H-2), 3.82 (1H, m, H-3), 3.62 (1H, t, *J*= 9.6 Hz, H-4), 3.86 (1H, m, H-5), 4.41 (1H, dd, *J*= 5.4, 12.0 Hz, H-6a), 4.67 (1H, dd, *J*= 1.8, 12.0 Hz, H-6b), 7.01 (2H, s, H-2′, 6′), 7.05 (2H, s, H-2″, 6″), 7.22 (1H, d, *J*= 1.8 Hz, H-2‴), 7.23 (1H, d, *J*= 1.8 Hz, H-6‴), 3.89 (3H, s, OMe); ^{13}C NMR (MeOH-d_4, 150 MHz) δ_C 94.1 (C-1), 74.2 (C-2), 76.1 (C-3), 71.7 (C-4), 76.6 (C-5), 64.6 (C-6), 120.0 (C-1′), 110.5 (C-2′, 6′), 146.5 (C-3′, 5′), 140.6 (C-4′), 166.5 (C-7′), 121.1 (C-1″), 110.4 (C-2″, 6″), 146.4 (C-3″, 5″), 140.0 (C-4″), 167.6 (C-7″), 121.3 (C-1‴), 106.3 (C-2‴), 149.2 (C-3‴), 140.7 (C-4‴), 146.3 (C-5‴), 112.0 (C-6‴), 168.1 (C-7‴), 56.7 (OMe); HRESIMS *m/z* 649.1051 $[M-H]^-$ (calcd for $C_{28}H_{25}O_{18}$, 649.1046).

4.4. Acid hydrolysis and GC/MS

Compound **20** (2.0 mg) and 1 mL HCl 1N in MeOH were stirred for 3 h at 60 °C in a sand bath. The reaction mixture was neutralized with sodium bicarbonate and partitioned with

EtOAc (3 times × 1 mL); the water layer was dried to obtain 0.7 mg of sugar fraction for analysis.

The sugar fraction was derivatized with L-cysteine methyl ester hydrochloride (1.5 mg in 200 μL pyridine, 60 °C, 1 h), subsequently silylated with BSTFA and TMCS (99:1, v/v) (200 μL, 60 °C, 1 h), and then analyzed by GC-MS. Reference compounds D-glucose (t_R= 77.31 min) and L-glucose (t_R= 77.59 min) were derivatized and analyzed using the same protocol. D-glucose was detected in **20**. GC-MS analyses were carried out on an Agilent 5975C Series GC/MSD System comprising a 7693 autosampler, a Triple AxisDetector (MS), and a 7890A GC. An Agilent HP-5MS column (30 m × 250 μm × 0.25 μm) was used for analysis, the other settings were as follows: temperature gradient: 70 °C for 2 min, then 2 °C/min to 150 °C (hold 150 °C for 2 min), then 5 °C/min to 220 °C (hold 220 °C for 15 min), then 15 °C/min to 300 °C (hold 300 °C for 10 min); total run time: 88 min; injection volume: 1 μL; split ratio 10:1; carrier gas: helium; flow rate: 7.5 mL/min.

4.5. Calculation of ECD spectra

The 3D structure of selected compounds was subjected to MacroModel 9.1 (Schrödinger. LLC, USA) to perform conformational analysis (parameters: MMFF force field; gas phase; maximum iterations: 10,000; maximum number of steps: 10,000; energy window: 5 kcal/mol). Conformers occurring in an energy window of 5 kcal/mol were subjected to geometry optimization and energy calculation using first DFT/B3LYP/6-31G (d) in the gas phase and then DFT/B3LYP/6-31G+(d,p)/CPCM in acetonitrile with Gaussian 16 (M. J. Frisch et al., 2016). No imaginary frequencies were observed for the optimized structures. Calculation of excitation energy (nm), rotatory strength, dipole velocity (R_{vel}) and dipole length (R_{len}) were performed by TD-DFT/cam-B3LYP/6-31G+(d,p)/CPCM (acetonitrile) for **1-3** and **8**, and TD-DFT/B3LYP/6-31G+(d,p)/CPCM (acetonitrile) for **4** and **5**. ECD curves were extracted by SpecDis v.1.7 software with a half-band of 0.2-0.3 eV (Bruhn et al., 2017). The Boltzmann-averaged ECD spectra were shifted ± 25 nm in the UV range, and then compared with the experimental results.

4.6. Calculation of NMR chemical shifts and DP4+ probability analysis

Diastereomers of **1**, **2** and **5** were subjected to conformational analysis in the gas phase (as mentioned in section 4.5). The conformers occurring in the energy window of 5 kcal/mol were subjected to geometry optimization using DFT/B3LYP/6-31G(d) in the gas phase with Gaussian 16. NMR chemical shift calculations were performed using GIAO/mPW1PW91/6-

31G+(d,p)/CPCM/chloroform, shielding tensors of all conformers were Boltzmann averaged and used for DP4+ probability calculation using the excel file provided by Grimblat's group (Grimblat et al., 2015).

4.7. AGEs inhibition assay

Inhibition of pentosidine-like AGEs formation was measured according to a previously published protocol (Séro et al., 2013). In short, depending on available sample material, stock solutions (SS) were prepared in DMSO at concentrations of 10 or 30 mM, respectively. These SS were then diluted with 50 mM phosphate buffer (pH: 7.4) yielding working solutions (WS) at a concentration range of 10^{-5} to 3.10^{-2} mol/L. Ten microliter of each WS were deposited in 96 black well bottom plates (Fisher Scientific, Illkirch, France) and mixed with 90 μL of a solution containing BSA (11 mg/L), D-ribose (0.55 M), and phosphate buffer (50 mM, NaN_3 0.02%, pH 7.4). Plates were then incubated for 24 h at 37°C before measuring their fluorescence (λ_{exc}: 335 nm, λ_{em}: 385 nm) using an Infinite M200 plate reader (Tecan, Lyon, France). Fluorescence resulting from the incubation, under the same BSA (final concentration: 10 mg/mL) and tested compound (10^{-6} to 3.10^{-3} mol/L) concentrations, was subtracted for each measurement. The control, *i.e*. no inhibition of AGEs formation, consisted of BSA (10 mg/mL) and D-ribose (0.5 M). Results (table 1) are expressed as IC_{50} (mM) and compared with aminoguanidine (positive control). Samples exhibiting an IC_{50} of more than 1 mM were considered inactive. Dimethyl sulfoxide served as negative control and was processed the same way as the WS.

Declaration of competing interest

The authors declare no competing financial interest.

Acknowledgments

This study was part of the project "China-TCM cluster" and financially supported by the Austrian Federal Ministry of Health and the Austrian Federal Ministry of Science, Research and Economy (BMWFW-402.000/0016-WF/V/6/2016).

Appendix A. Supplementary data

Supplementary data (including 1D and 2D-NMR spectra, HRESIMS, and DP4+ probability analyses of previously undescribed compounds) to this article can be found online.

589 **References**

590

591 Abdullaeva, R. K., Bobakulov, K. M., Nishanbaev, C. Z., Sham′yanov, I. D., Abdullaev, N. D.,
592 2016. Flavonoids and other constituents from the aerial part of *Anaphalis racemifera*. Chem.
593 Nat. Compd. 52, 503-504. https://doi.org/10.1007/s10600-016-1688-2.

594 An, J. P., Ha, T. K., Kim, J., Cho, T. O., Oh, W. K., 2016. Protein tyrosine phosphatase 1B
595 inhibitors from the stems of *Akebia quinata*. Molecules 21.
596 https://doi.org/10.3390/molecules21081091.

597 Asia Foundation, 2012. Guide to medicinal plants of Daos in Ba Vi,
598 https://asiafoundation.org/resources/pdfs/MedicinalPlantIndexoftheDaosinBaVi.pdf

599 Bicker, J., Petereit, F., Hensel, A., 2009. Proanthocyanidins and a phloroglucinol derivative
600 from *Rumex acetosa* L. Fitoterapia 80, 483-495. https://doi.org/10.1016/j.fitote.2009.08.015.

601 Bouzergoune, F., Ciavatta, M. L., Bitam, F., Carbone, M., Aberkane, M. C., Gavagnin, M.,
602 2016. Phytochemical study of *Eryngium triquetrum*: Isolation of polyacetylenes and lignans.
603 Planta Med. 82, 1438-1445. https://doi.org/10.1055/s-0042-110316.

604 Bozzo, C., Pujol, M. D., Solans, X., Font-Bardia, M., 2003. A new synthesis of 3-hydroxy-2,3-
605 dihydro-1,4-benzodioxin-2-carboxamides and 3-aminomethylene-1,4-benzodioxin-2(3H)-one
606 derivatives. Tetrahedron 59, 1227-1236. https://doi.org/10.1016/S0040-4020(03)00025-5.

607 Bringmann, G., Rischer, H., Wohlfarth, M., Schlauer, J., 2000a. Biosynthesis of antidesmone
608 in cell cultures of *Antidesma membranaceum* (Euphorbiaceae): An unprecedented class of
609 glycine-derived alkaloids. J. Am. Chem. Soc. 122, 9905-9910.
610 https://doi.org/10.1021/ja001391k.

611 Bringmann, G., Schlauer, J., Rischer, H., Wohlfarth, M., Mühlbacher, J., Buske, A., Porzel, A.,
612 Schmidt, J., Adam, G., 2000b. Revised structure of antidesmone, an unusual alkaloid from
613 tropical *Antidesma* plants (Euphorbiaceae). Tetrahedron 56, 3691-3695.
614 https://doi.org/10.1016/S0040-4020(00)00289-1.

615 Bruhn, T., Schaumlöffel, A., Hemberger, Y., Pecitelli, G., 2017. SpecDis, Version 1.70. Berlin,
616 Germany.

617 Buske, A., Schmidt, J., Porzel, A., Adam, G., 2001. Alkaloidal, megastigmane and lignan
618 glucosides from *Antidesma membranaceum* (Euphorbiaceae). European J. Org. Chem. 18,
619 3537-3543. https://doi.org/10.1002/1099-0690(200109)2001:18%3C3537::AID-
620 EJOC3537%3E3.0.CO;2-A.

621 Cai, Y., Cai, T.-G., 2010. Two new aristolochic acid derivatives from the roots of *Aristolochia*
622 *fangchi* and their cytotoxicities. Chem. Pharm. Bull 58, 1093-1095.
623 https://doi.org/10.1248/cpb.58.1093.

624 Caro, M. S. B., de Oliveira, L. H., Ilha, V., Burrow, R. A., Dalcol, I. I., Morel, A. F., 2012.
625 Absolute configuration of franganine. J. Nat. Prod. 75, 1220-1222.
626 https://doi.org/10.1021/np300206x.

627 Chen, Y.-C., Cheng, M.-J., Lee, S.-J., Dixit, A. K., Ishikawa, T., Tsai, I.-L., Chen, I.-S., 2004.
628 Coumarinolignans from the root of Formosan *Antidesma pentandrum* var. barbatum. Helv.
629 Chim. Acta. 87, 2805-2811. https://doi.org/10.1002/hlca.200490251.

630 Chen, Y.-C., Cheng, M.-J., Lee, S.-J., Tsai, I.-L., Chen, I.-S., 2007. Chemical constituents from
631 the root of *Antidesma pentandrum* var. *barbatum*. J. Chin. Chem. Soc. 54, 1325-1332.
632 https://doi.org/10.1002/jccs.200700187.

633 Cretton, S., Breant, L., Pourrez, L., Ambuehl, C., Marcourt, L., Ebrahimi, S. N., Hamburger,
634 M., Perozzo, R., Karimou, S., Kaiser, M., Cuendet, M., Christen, P., 2014. Antitrypanosomal
635 quinoline alkaloids from the roots of *Waltheria indica*. J. Nat. Prod. 77, 2304-2311.
636 https://doi.org/10.1021/np5006554.

637 Dariya, B., Nagaraju, G. P., 2020. Advanced glycation end products in diabetes, cancer and
638 phytochemical therapy. Drug Discov. Today 25, 1614-1623.
639 https://doi.org/10.1016/j.drudis.2020.07.003.

640 Darwish, F. M. M., Reinecke, M. G., 2003. Ecdysteroids and other constituents from *Sida*
641 *spinosa* L. Phytochemistry 62, 1179-1184. https://doi.org/10.1016/S0031-9422(03)00021-9.

642 De Groot, L., Posthumus, M. D., Kallenberg, C. G. M., Bijl, M., 2010. Risk factors and early
643 detection of atherosclerosis in rheumatoid arthritis. Eur. J. Clin. Invest. 40, 835-842.
644 https://doi.org/10.1111/j.1365-2362.2010.02333.x.

eFloras, 2008. Published on the Internet http://www.efloras.org [accessed January 2022] Missouri Botanical Garden, St. Louis, MO & Harvard University Herbaria, Cambridge, MA.

Gerards, M., Snatzke, G., 1990. Circular dichroism, XCIII determination of the absolute configuration of alcohols, olefins, epoxides, and ethers from the CD of their "in situ" complexes with [Rh2(O_2CCF_3)$_4$]. Tetrahedron: Asymmetry 1, 221-236. https://doi.org/10.1016/S0957-4166(00)86328-4.

Grimblat, N., Zanardi, M. M., Sarotti, A. M., 2015. Beyond DP4: an improved probability for the stereochemical assignment of isomeric compounds using quantum chemical calculations of NMR shifts. J. Org. Chem. 80, 12526-12534. https://doi.org/10.1021/acs.joc.5b02396.

Han, B. H., Park, M. H., Han, Y. N., 1990. Cyclic peptide and peptide alkaloids from seeds of *Zizyphus vulgaris*. Phytochemistry 29, 3315-3319. https://doi.org/10.1016/0031-9422(90)80207-W.

Hiltunen, E., Pakkanen Tuula, T., Alvila, L., 2006. Phenolic compounds in silver birch (*Betula pendula* Roth) wood. hfsg 60, 519. https://doi.org/10.1515/HF.2006.086.

Khan, M., Liu, H., Wang, J., Sun, B., 2020. Inhibitory effect of phenolic compounds and plant extracts on the formation of advance glycation end products: A comprehensive review. Food Res. Int. 130, 108933. https://doi.org/10.1016/j.foodres.2019.108933.

Kiyekbayeva, L., Mohamed, N. M., Yerkebulan, O., Mohamed, E. I., Ubaidilla, D., Nursulu, A., Assem, M., Srivedavyasasri, R., Ross, S. A., 2018. Phytochemical constituents and antioxidant activity of *Echinops albicaulis*. Nat. Prod. Res. 32, 1203-1207. https://doi.org/10.1080/14786419.2017.1323213.

Krongyut, O., Sutthanut, K., 2019. Phenolic profile, antioxidant activity, and anti-obesogenic bioactivity of Mao Luang fruits (*Antidesma bunius* L.). Molecules 24, 4109. https://doi.org/10.3390/molecules24224109.

Lee, S.-J., Jang, H.-J., Kim, Y., Oh, H.-M., Lee, S., Jung, K., Kim, Y.-H., Lee, W.-S., Lee, S.-W., Rho, M.-C., 2016. Inhibitory effects of IL-6-induced STAT3 activation of bio-active compounds derived from *Salvia plebeia* R.Br. Process Biochem. 51, 2222-2229. https://doi.org/10.1016/j.procbio.2016.09.003.

673 Lomchoey, N., Panseeta, P., Boonsri, P., Apiratikul, N., Prabpai, S., Kongsaeree, P.,
674 Suksamrarn, S., 2018. New bioactive cyclopeptide alkaloids with rare terminal unit from the
675 root bark of *Ziziphus cambodiana*. RSC Adv. 8, 18204-18215.
676 https://doi.org/10.1039/C7RA13050C.

677 Lu, Y., Xue, Y., Liu, J., Yao, G., Li, D., Sun, B., Zhang, J., Liu, Y., Qi, C., Xiang, M., Luo, Z.,
678 Du, G., Zhang, Y., 2015. (±)-Acortatarinowins A–F, norlignan, neolignan, and lignan
679 enantiomers from *Acorus tatarinowii*. J. Nat. Prod. 78, 2205-2214.
680 https://doi.org/10.1021/acs.jnatprod.5b00328.

681 M. J. Frisch, G. W. Trucks, H. B. Schlegel, G. E. Scuseria, M. A. Robb, J. R. Cheeseman, G.
682 Scalmani, V. Barone, G. A. Petersson, H. Nakatsuji, X. Li, M. Caricato, A. Marenich, J. Bloino,
683 B. G. Janesko, R. Gomperts, B. Mennucci, H. P. Hratchian, J. V. Ortiz, A. F. Izmaylov, J. L.
684 Sonnenberg, D. Williams-Young, F. Ding, F. Lipparini, F. Egidi, J. Goings, B. Peng, A.
685 Petrone, T. Henderson, D. Ranasinghe, V. G. Zakrzewski, J. Gao, N. Rega, G. Zheng, W. Liang,
686 M. Hada, M. Ehara, K. Toyota, R. Fukuda, J. Hasegawa, M. Ishida, T. Nakajima, Y. Honda, O.
687 Kitao, H. Nakai, T. Vreven, K. Throssell, J. A. Montgomery, J., J. E. Peralta, F. Ogliaro, M.
688 Bearpark, J. J. Heyd, E. Brothers, K. N. Kudin, V. N. Staroverov, T. Keith, R. Kobayashi, J.
689 Normand, K. Raghavachari, A. Rendell, J. C. Burant, S. S. Iyengar, J. Tomasi, M. Cossi, J. M.
690 Millam, M. Klene, C. Adamo, R. Cammi, J. W. Ochterski, R. L. Martin, K. Morokuma, O.
691 Farkas, J. B. Foresman, Fox, D. J., 2016. Gaussian 16. Gaussian, Inc., Wallingford CT.

692 Martin, F., Hay, A.-E., Cressend, D., Reist, M., Vivas, L., Gupta, M. P., Carrupt, P.-A.,
693 Hostettmann, K., 2008. Antioxidant C-glucosylxanthones from the leaves of *Arrabidaea*
694 *patellifera*. J. Nat. Prod. 71, 1887-1890. https://doi.org/10.1021/np800406q.

695 Mauldina, M. G., Sauriasari, R., Elya, B., 2017. α-glucosidase inhibitory activity from ethyl
696 acetate extract of *Antidesma bunius* (L.) Spreng stem bark containing triterpenoids.
697 Pharmacogn Mag 13, 590-594. https://doi.org/10.4103/pm.pm_25_17.

698 Nagaraj, R. H., Shipanova, I. N., Faust, F. M., 1996. Protein cross-linking by the Maillard
699 reaction. Isolation, characterization, and in vivo detection of a lysine-lysine cross-link derived
700 from methylglyoxal. The Journal of biological chemistry 271, 19338-19345.
701 https://doi.org/10.1074/jbc.271.32.19338.

702 Ngamlerst, C., Udomkasemsab, A., Kongkachuichai, R., Kwanbunjan, K., Chupeerach, C.,
703 Prangthip, P., 2019. The potential of antioxidant-rich Maoberry (*Antidesma bunius*) extract on

fat metabolism in liver tissues of rats fed a high-fat diet. BMC Complement. Altern. Med. 19, 294. https://doi.org/10.1186/s12906-019-2716-0.

Owen, R. W., Haubner, R., Hull, W. E., Erben, G., Spiegelhalder, B., Bartsch, H., Haber, B., 2003. Isolation and structure elucidation of the major individual polyphenols in carob fibre. Food Chem. Toxicol. 41, 1727-1738. https://doi.org/10.1016/S0278-6915(03)00200-X.

Peng, W. C., 2011. Constituents from charred *Cirsium japonicum*. Chem. Nat. Compd. 47, 279. https://doi.org/10.1007/s10600-011-9904-6.

Rouger, C., Derbré, S., Charreau, B., Pabois, A., Cauchy, T., Litaudon, M., Awang, K., Richomme, P., 2015. Lepidotol A from *Mesua lepidota* inhibits inflammatory and immune mediators in human endothelial cells. J. Nat. Prod. 78, 2187-2197. https://doi.org/10.1021/acs.jnatprod.5b00222.

Séro, L., Sanguinet, L., Blanchard, P., Dang, B. T., Morel, S., Richomme, P., Séraphin, D., Derbré, S., 2013. Tuning a 96-well microtiter plate fluorescence-based assay to identify AGE inhibitors in crude plant extracts. Molecules 18, 14320-14339. https://doi.org/10.3390/molecules181114320.

Shao, S.-Y., Yang, Y.-N., Feng, Z.-M., Jiang, J.-S., Zhang, P.-C., 2018. An efficient method for determining the relative configuration of furofuran lgnans by 1H NMR spectroscopy. J. Nat. Prod. 81, 1023-1028. https://doi.org/10.1021/acs.jnatprod.8b00044.

Tanaka, T., Fujisaki, H., Nonaka, G.-i., Nishioka, I., 1992. Tannins and related compounds. CXVIII. Structures, preparation, high-performance liquid chromatography and some reactions of dehydroellagitannin-acetone condensates. Chem. Pharm. Bull 40, 2937-2944. https://doi.org/10.1248/cpb.40.2937.

Tanaka, T., Nonaka, G.-I., Nishioka, I., 1985. Punicafolin, an ellagitannin from the leaves of *Punica granatum*. Phytochemistry 24, 2075-2078. https://doi.org/10.1016/S0031-9422(00)83125-8.

Tawali S, As'ad S, Hatta M, Bukhari A, Khairi N, Rifai Y, R, D., 2019. Anthocyanin-rich buni-berry (*Antidesma bunius*) extract increases paraoxonase 1 gene expression in BALB/c mice fed with a high-fat diet. J. Young Pharm. 11, 46-50. https://doi.org/10.5530/jyp.2019.11.10.

732 Torres-Tapia, L. W., Sosa-Espinosa, T., Peraza-Sánchez, S. R., 2013. Isolation of a p-
733 hydroxyphenyl anhydride from the leaves of *Diphysa carthagenensis*. Nat. Prod. Res. 27, 286-
734 289. https://doi.org/10.1080/14786419.2012.668689.

735 Trang, D. T., Huyen, L. T., Nhiem, N. X., Quang, T. H., Hang, D. T. T., Yen, P. H., Tai, B. H.,
736 Anha, H. L. T., Binh, N. Q., Van Minha, C., Van Kiem, P., 2016. Tirucallane glycoside from
737 the leaves of *Antidesma bunius* and inhibitory NO production in BV2 cells and RAW264.7
738 macrophages. Nat Prod Commun 11, 935-937. https://doi.org/10.1177/1934578X1601100717.

739 Ueno, Y., Kato, Y., Okatani, S., Ishida, N., Nakanishi, M., Kitade, Y., 2003. Synthesis of
740 antisense oligonucleotides carrying modified 2-5A molecules at their 5‘-termini and their
741 properties. Bioconjug. Chem. 14, 690-696. https://doi.org/10.1021/bc020072a.

742 Xiong, L., Zhu, C., Li, Y., Tian, Y., Lin, S., Yuan, S., Hu, J., Hou, Q., Chen, N., Yang, Y., Shi,
743 J., 2011. Lignans and neolignans from *Sinocalamus affinis* and their absolute configurations. J.
744 Nat. Prod. 74, 1188-1200. https://doi.org/10.1021/np200117y.

745 Yoshida, T., Hatano, T., Okuda, T., Memon, M. U., Shingu, T., Inoue, K., 1984. Spectral and
746 chromatographic analyses of tnnins. I. 13C Nuclear Magnetic Resonance spectra of
747 hydrolyzable tannins. Chem. Pharm. Bull 32, 1790-1799. https://doi.org/10.1248/cpb.32.1790.

748

749

750

751 **Figure and Table legends**

752

753 Fig. 1. Chemical structures of isolated compounds from *A. bunius* aerial parts.

754 Fig. 2. Key HMBC (H→C) and ^{1}H-^{1}H COSY correlations of compounds **1**-**5**, **8**, **16**, **17**, and **20**.

755 Fig. 3. Experimental CD spectra of **1** and **2**; (B-F) Calculated and experimental ECD spectra
756 of **2**, **3**, **4**, **5**, and **8**.

757

758 Table 1. NMR spectroscopic data (600 MHz, $CDCl_3$) for compounds **1**-**3**.

759 Table 2. NMR spectroscopic data (600 MHz, $CDCl_3$) for compounds **4** and **5**.

760 Table 3. NMR spectroscopic data (600 MHz, $CDCl_3$) for compounds **16** and **17**.

761 Table 4. Anti-AGEs activity of selected natural products isolated from *A. bunius* aerial parts.

762

763 Fig.1

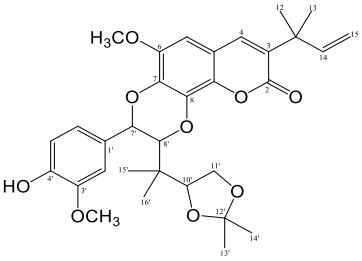

1 7′*R*, 8′*R*, 10′*R*
2 7′*S*, 8′*S*, 10′*R*

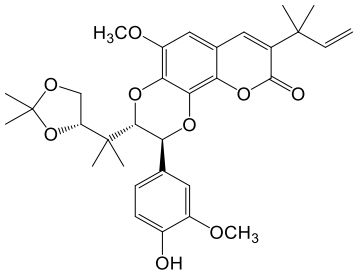

3

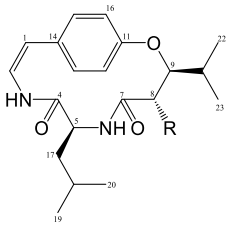

R

4 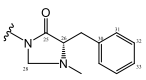

6 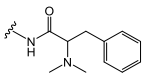

7 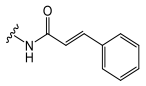

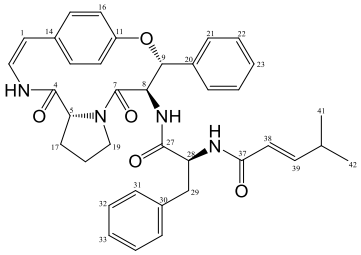

5

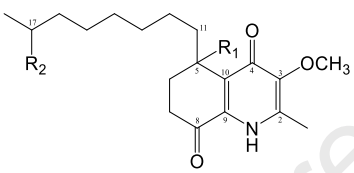

	R_1	R_2
8	α-OH	H
9	β-H	H
10	β-H	*O*-glc

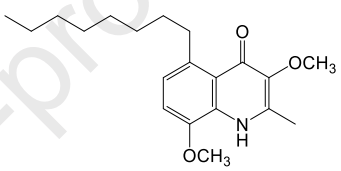

11

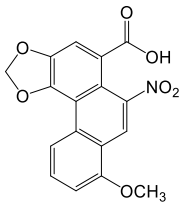

12

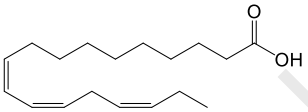

13

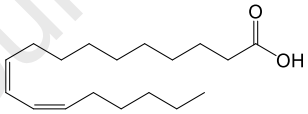

14

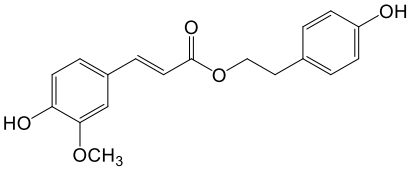

15

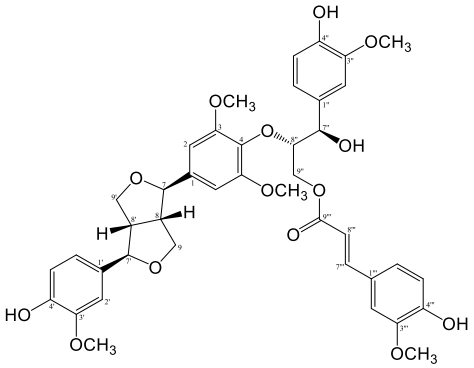

16

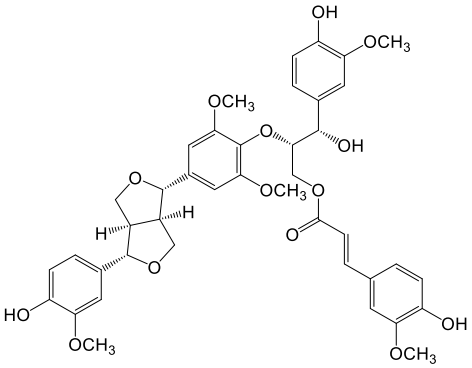

17

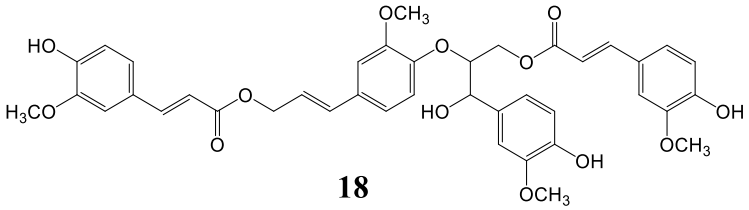

18

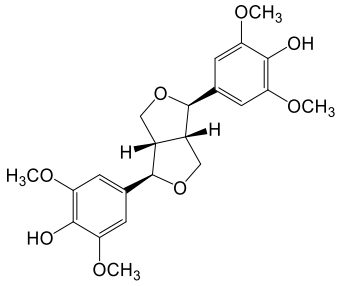

19

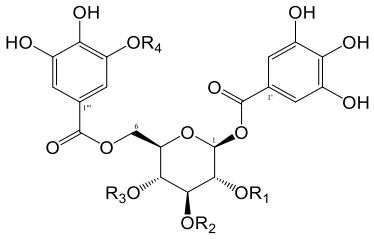

	R_1	R_2	R_3	R_4
20	G	H	H	CH_3
21	H	G	H	H
22	H	H	G	H

G = 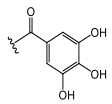

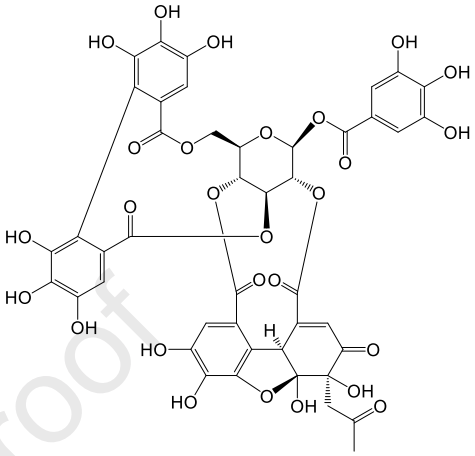

23

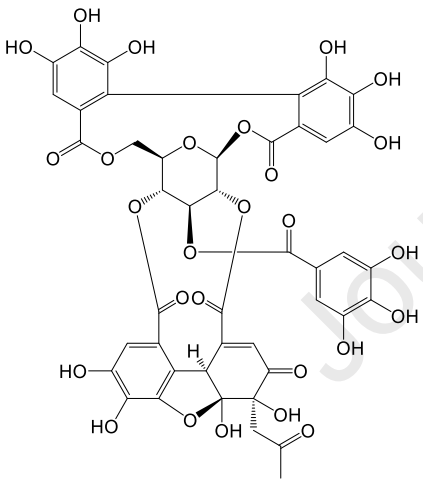

24

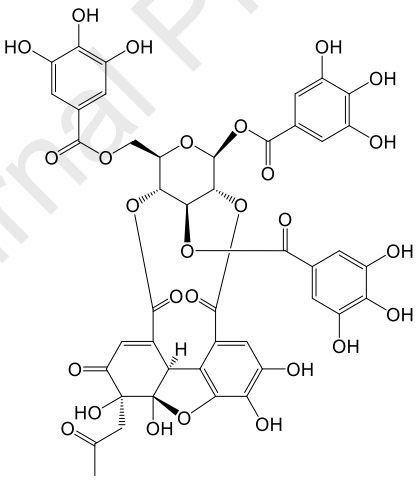

25

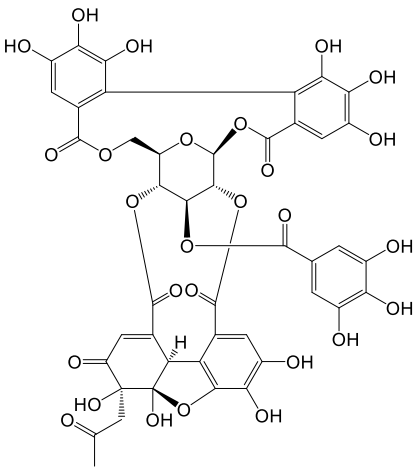

26

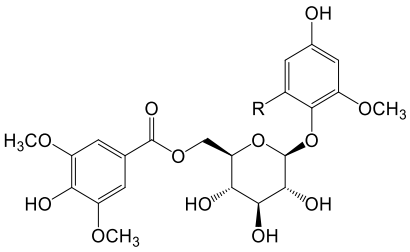

	R
27	OH
28	H

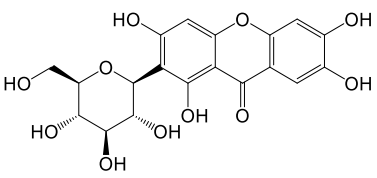

29

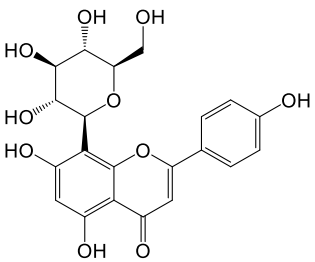

33

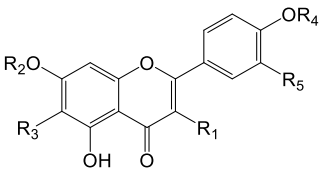

	R_1	R_2	R_3	R_4	R_5
30	*O*-rha	H	H	H	OH
31	*O*-glc(6→1)rha	H	H	H	OH
32	H	*O*-glc(6→1)rha	OCH_3	CH_3	H

764

765

766

767 Fig. 2

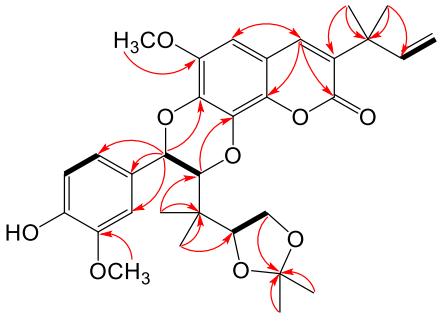

1, **2**

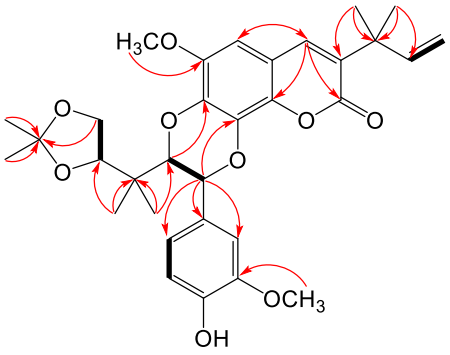

3

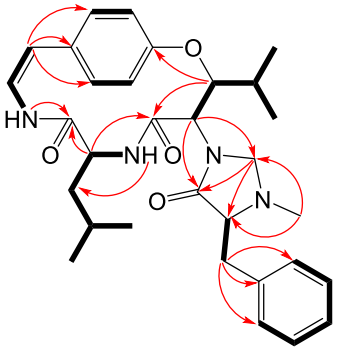

4

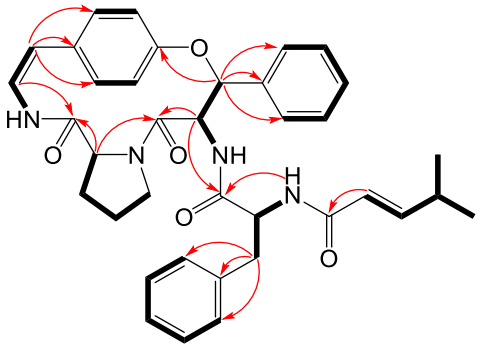

5

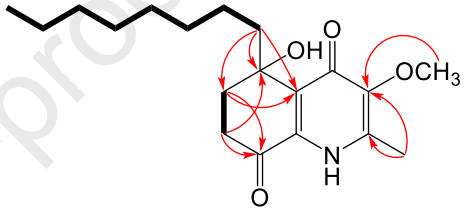

8

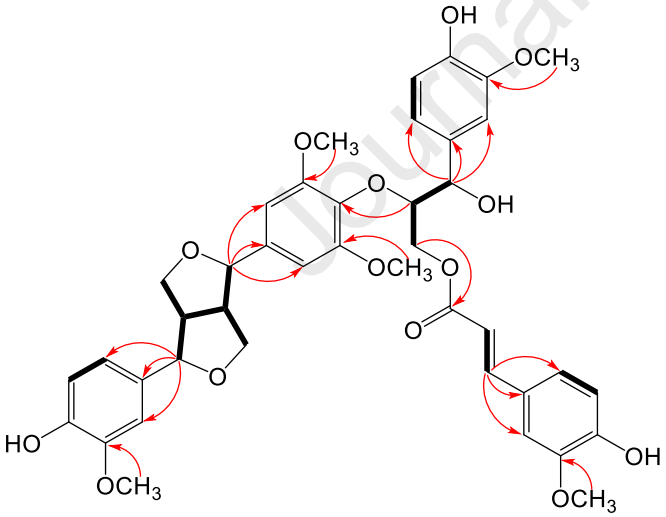

16, **17**

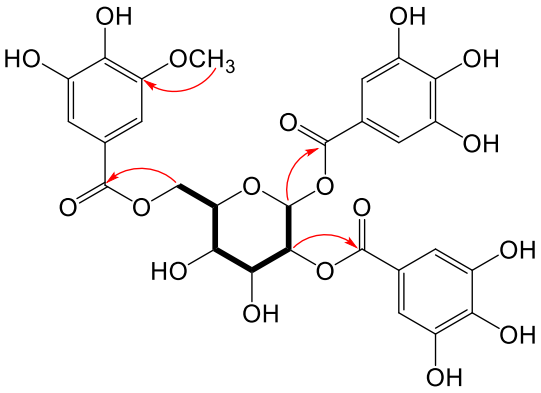

20

HMBC
COSY

768

769

770 Fig. 3

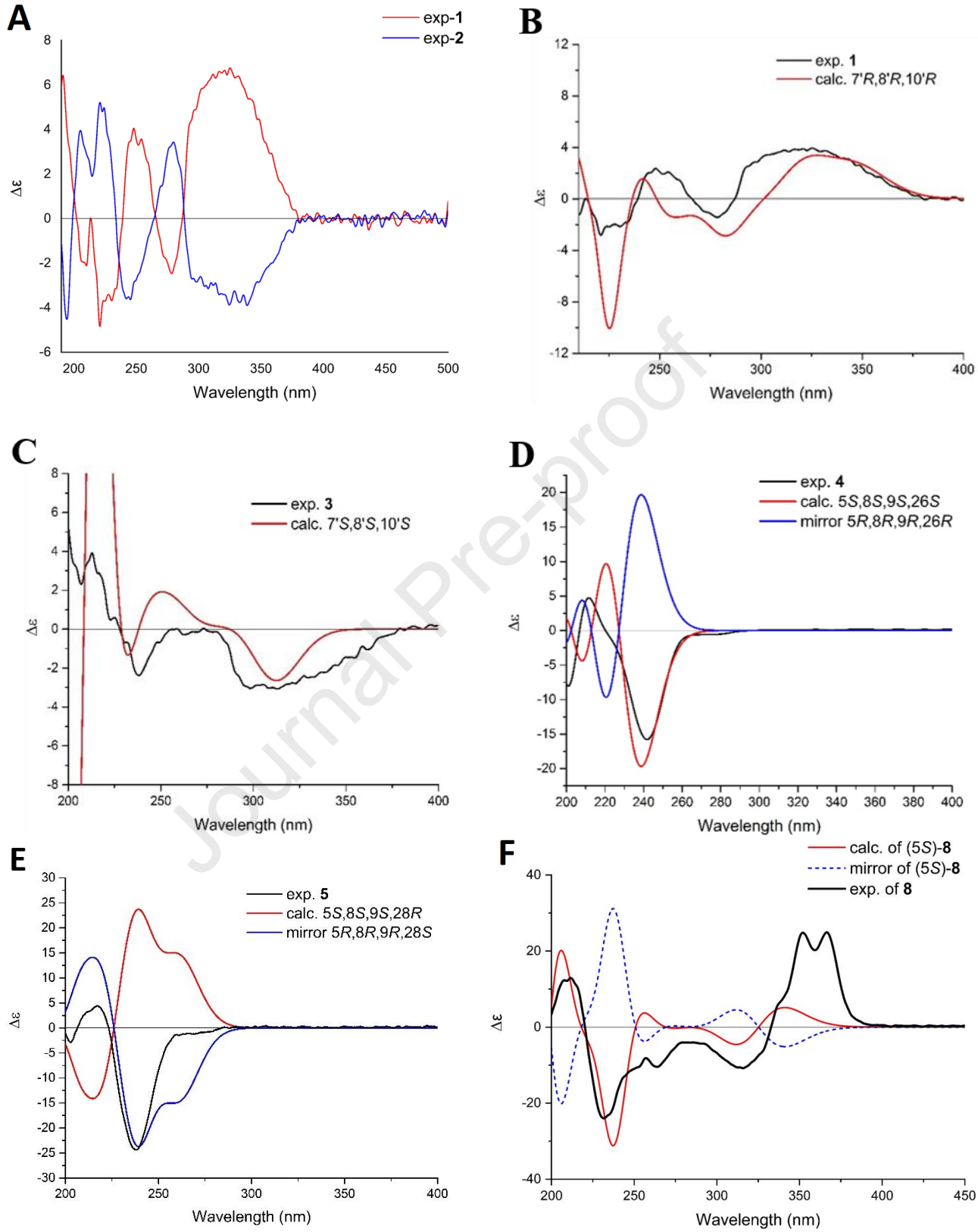

771

772

773 Table 1

position	**1**		**2**		**3**	
2	159.9		159.9		160.1	
3	132.8		132.8		132.6	
4	138.1	7.46, s	138.2	7.48, s	138.2	7.45, s
5	100.0	6.45, s	100.0	6.47, s	100.7	6.47, s
6	145.7		145.6		145.8	
7	135.7		136.5		136.5	
8	132.0		132.0		131.2	
9	137.9		138.2		138.2	
10	112.3		112.0		111.8	
11	40.7		40.7		40.6	
12[a]	26.2	1.48, s	26.2	1.49, s	26.2	1.45, s
13[a]	26.2	1.48, s	26.2	1.49, s	26.2	1.45, s
14	145.8	6.18, dd (10.2, 17.4)	145.8	6.19, dd (10.2, 17.4)	145.8	6.15, dd (10.2, 17.4)
15	112.1	5.09, d (12.0)	112.3	5.09, d (12.0)	112.3	5.06, d (10.2)
		5.09, d (17.4)		5.09, d (17.4)		5.07, d (17.4)
1′	129.6		129.3		129.5	
2′	110.6	6.91, d (1.8)	111.2	6.93, d (1.8)	110.6	6.92, m
3′	146.9		146.7		146.9	
4′	146.5		146.5		146.5	
5′	114.7	6.89, d (8.4)	114.4	6.89, d (8.4)	114.5	6.87, d (8.4)
6′	121.6	6.94, dd (1.8, 8.4)	122.4	6.96, dd (1.8, 8.4)	121.3	6.92, m
7′	76.4	5.22, d (5.4)	77.8	5.15, d (6.6)	75.4	5.22, d (4.8)
8′	80.3	4.36, d (5.4)	82.2	4.16, d (6.6)	80.7	4.36, d (4.8)
9′	40.7		40.3		40.9	
10′	79.5	4.44, t (7.2)	77.9	4.14, t (7.2)	80.1	4.29, t (7.2)
11′	65.4	3.79, dd (7.2, 8.4)	65.2	3.70, t (8.4)	65.8	3.78, t (8.4)
		4.09, dd (7.2, 8.4)		3.90, m		4.11, dd (6.6, 8.4)
12′	108.9		108.9		108.3	
13′[b]	25.1	1.35, s	25.4	1.27, s	25.2	1.34, s
14′[b]	26.4	1.38, s	26.5	1.37, s	26.5	1.38, s
15′[c]	17.5	0.97, s	19.4	0.87, s	17.0	0.97, s
16′[c]	19.3	0.72, s	21.2	0.95, s	20.0	0.76, s
6-OMe	56.5	3.84, s	56.4	3.84, s	56.6	3.87, s
3′-OMe	56.2	3.87, s	56.1	3.89, s	56.2	3.87, s

774 [a,b,c] interchangeable signals

775

776 Table 2

position		**4**		**5**
1	116.7	6.40, d (9.6)	116.1	6.40, d (7.8)
2	125.9	6.65, dd (8.4, 9.6)	125.7	6.74, d (7.8)
3		6.38 (d, 8.4)		6.57, d (8.4)
4	167.4		166.5	
5	52.8	4.04, m	59.2	3.85, d (7.2)
6		5.44, d (7.8)		
7	168.3		170.6	
8	57.0	4.55, d (7.8)	56.0	4.74, dd (7.2, 10.2)
9	80.6	4.85, dd (1.8, 7.8)	82.1	5.93, d (7.2)
11	156.1		155.5	
12	122.5	7.15, dd (2.4, 8.4)	123.7	7.36, m
13	131.6	7.04, m	132.1	7.12, m
14	132.0		132.8	
15	130.6	7.03, m	130.5	7.07, m
16	123.0	7.11, dd (2.4, 8.4)	123.7	7.24, m
17	39.2	1.31, ddd (3.0, 12.0, 15.0)	26.1	1.39, m
		1.78, ddd (3.0, 10.2, 15.0)		2.17, m
18	24.5	1.21, m	24.6	1.45, m
				1.77, m
19	21.2	0.73, d (6.6)	46.9	2.90, t (8.4)
				3.10, dt (6.6, 12.0)
20	23.5	0.86, d (6.6)	137.5	
21	28.9	1.50, m	128.4	7.35, m
22	14.7	0.68, d (6.6)	128.5	7.24, m
23	20.7	1.14, d (7.2)	128.4	7.24, m
24			128.5	7.24, m
25	172.4		128.4	7.35, m
26	67.5	2.85, m		7.41, d, 9.6
27			170.9	
28	68.4	3.25, dd (1.8, 5.4)	54.3	4.54, m
		4.07, d (5.4)		
29	35.9	2.94, dd (5.4, 14.4)	36.2	2.81, dd (10.2, 15.0)
		3.11, dd (4.2, 14.4)		3.32, dd (1.8, 15.0)
30	137.2		136.4	
31,35	130.2	7.24, m	128.8	7.06, m
32,34	128.3	7.27, m	128.9	7.21, m
33	126.7	7.22, m	126.9	7.11, m
36				5.80, d (7.8)
37			166.5	
38			117.9	5.64, d (15.0)
39			153.9	6.76, dd (6.6, 15.0)
40			31.3	2.49, m
41			21.6	1.14, d (6.6)
42			21.6	1.11, d (7.2)
N-Me	39.3	2.22, s		

777

778

779 Table 3

position	**16**		**17**	
1	137.9		137.8	
2, 6	103.0	6.61, s	102.7	6.58, s
3, 5	153.8		153.0	
4	134.1		135.9	
7	86.2	4.74, d (5.4)	86.1	4.73, t (4.8)
8	54.7	3.08, m	54.7	3.06, m
9	71.7	3.91, m	71.7	3.90, m
		4.26, dd (6.6, 9.0)		4.26, dd (7.2, 9.0)
3, 5-OMe	56.4	3.87, s	56.2	3.87, s
1′	132.9		132.9	
2′	108.8	6.89, m	108.7	6.89, m
3′	146.9		146.6	
4′	145.5		145.4	
5′	114.4	6.89, m	114.4	6.89, m
6′	119.1	6.82, d (7.8)	119.1	6.82, dd (1.8, 7.8)
7′	85.9	4.76, d (5.4)	85.9	4.75, d (4.8)
8′	54.2	3.12, m	54.2	3.10, m
9′	72.3	3.91, m	72.2	3.91, m
		4.30, m		4.28, dd (7.2, 9.0)
3′-OMe	56.1	3.91, s	56.0	3.83, s
4′-OH		5.59, s		5.59, s
1″	130.9		131.7	
2″	108.6	7.02, m	109.5	6.88, m
3″	146.9		146.6	
4″	145.0		145.6	
5″	114.2	6.87, m	114.4	6.84, d (8.4)
6″	119.0	6.76, d (7.8)	120.3	6.89, m
7″	71.7	4.89, d (3.6)	74.4	5.10, d (8.4)
8″	83.4	4.56, dt (3.6, 7.2)	87.1	4.07, m
9″	62.6	4.33, m	63.8	4.01, m
		4.46, dd (8.4, 12.0)		4.53, dt (3.0, 12.6)
3″-OMe	56.1	3.92, s	56.1	3.95, s
4″-OH		5.53, s		5.53, s
7″-OH		4.21, dd (2.4, 7.8)		4.67, dd (1.8, 9.6)
1‴	127.2		127.2	
2‴	109.4	7.00, m	109.3	7.06, m
3‴	146.8		146.9	
4‴	148.1		148.2	
5‴	114.8	6.90, m	114.9	6.93, dd (1.8, 7.8)
6‴	123.2	7.03, m	123.4	7.07, m
7‴	144.9	7.51, dd (4.2, 15.6)	145.2	7.56, dd (12.0, 15.6)
8‴	115.7	6.24, dd (1.2, 15.6)	115.2	6.35, dd (3.0, 15.6)
9‴	167.2		167.1	
3‴-OMe	56.1	3.89, s	56.1	3.91, s
4‴-OH		5.83, s		5.87, s

780

781

782 Table 4

compound	**IC_{50} (mM)**
Frangufoline (**6**)	NA
Sanjoinenine (**7**)	NA
Antidesmone (**9**)	0.7
17-*O*-(β-D-glucopyranosyl)antidesmone acid (**10**)	1.0
Waltherione F (**11**)	[b]
p-hydroxyphenylethyl *trans*-ferulate (**15**)	0.15
1,3,6-tri-*O*-galloyl-β-D-glucopyranose (**21**)	NA
Acetonylgranatin B (**23**)	0.2
Acetonylhelioscopinin A (**24**)	0.2
Acetonylterchebin (**25**)	0.2
Acetonylcarpinusin (**26**)	0.2
1-*O*-β-D-(2,4-dihydroxy-6-methoxyphenyl)-6-*O*-(4-hydroxy-3,5-dimethoxybenzoyl)-glucopyranose (**27**)	0.5
Quercitrin (**30**)	0.2
Rutin (**31**)	0.10
Aminoguanidine[a]	1.4

783 [a]reference [b]strong fluorescence interferences, NA = not active but no fluorescence
784 interferences

785

Highlights

- A comprehensive phytochemical characterization of *Antidesma bunius* is presented.
- Nine undescribed natural products were among the 33 isolated compounds.
- They represent coumarinolignans, cyclopeptides and furofuran-type lignans.
- Their configuration was established by ECD experiments and NMR calculations.
- Some compounds indicated inhibition of advanced glycation endproducts formation.

Conflict of interest

- none

Declaration of interests

☒ The authors declare that they have no known competing financial interests or personal relationships that could have appeared to influence the work reported in this paper.

☐The authors declare the following financial interests/personal relationships which may be considered as potential competing interests: